Fisheries and Oceans Canada | Pêches et Océans Canada
Ecosystems and Oceans Science | Sciences des écosystèmes et des océans

Canadian Science Advisory Secretariat (CSAS)

Research Document 2024/074

Newfoundland and Labrador Region

Biogeochemical Oceanographic Conditions on the Newfoundland and Labrador Shelf during 2019 and 2020

D. Bélanger, G. Maillet, F. Cyr, G. Doyle, S. Rastin, D. Ramsay, B. Dalton and P. Pepin

Science Branch
Fisheries and Oceans Canada
PO Box 5667
St. John's, Newfoundland, Canada A1C 5X1

November 2024

Canada

Foreword

This series documents the scientific basis for the evaluation of aquatic resources and ecosystems in Canada. As such, it addresses the issues of the day in the time frames required and the documents it contains are not intended as definitive statements on the subjects addressed but rather as progress reports on ongoing investigations.

Published by:

Fisheries and Oceans Canada
Canadian Science Advisory Secretariat
200 Kent Street
Ottawa ON K1A 0E6

http://www.dfo-mpo.gc.ca/csas-sccs/
csas-sccs@dfo-mpo.gc.ca

© His Majesty the King in Right of Canada, as represented by the Minister of the Department of Fisheries and Oceans, 2024
ISSN 1919-5044
ISBN 978-0-660-74110-9 Cat. No. Fs70-5/2024-074E-PDF

Correct citation for this publication:

Bélanger, D., Maillet, G., Cyr, F., Doyle, G., Rastin, S., Ramsay, D., Dalton, B., and Pepin, P. 2024. Biogeochemical Oceanographic Conditions on the Newfoundland and Labrador Shelf during 2019 and 2020. DFO Can. Sci. Advis. Sec. Res. Doc. 2024/074. vi + 55 p.

Aussi disponible en français :

Bélanger, D., Maillet G., Cyr, F., Doyle, G., Rastin, S., Ramsay, D., Dalton, B., et Pepin, P. 2024. Conditions océanographiques biogéochimiques sur le plateau continental de Terre-Neuve-et-Labrador en 2019 et 2020. Secr. can. des avis sci. du MPO. Doc. de rech. 2024/074 . vii + 58 p.

TABLE OF CONTENTS

LIST OF TABLES

LIST OF FIGURES

ABSTRACT

Biogeochemical oceanographic conditions in the Newfoundland and Labrador (NL) Region in 2019 and 2020 are presented and compared to long-term average conditions. Satellite observations indicated a general shift toward earlier onset of the spring phytoplankton bloom across the Region compared to the mid-to-late 2010s period with mixed effects on bloom magnitudes. The mainly near- or above-normal deep (50–150 m) nutrient inventories represented an increase compared to 2017 and 2018. Integrated (0–100 m) chlorophyll *a* (Chl *a*) biomass was mostly above normal across the region in 2019 continuing a trend that started in 2017, but declined to near-normal levels everywhere except on the Seal Island (SI) section in 2020. Total abundance of copepods and non-copepod zooplankton continued to be higher than normal in 2019 and 2020 with several record-high values for the Newfoundland Shelf in 2020. Total zooplankton biomass was below normal on the southeastern Grand Bank (SEGB) in 2019, higher than normal on the Newfoundland Shelf in 2020, and otherwise near normal elsewhere in both years. The abundance of large *Calanus finmarchicus* copepods decreased to below-normal levels on most of the Grand Bank in 2020 after having remained mostly near or above normal from 2017 to 2019. In contrast, the overall abundance of small copepod taxa remained high with several record-high values for *Pseudocalanus* spp. and *Oithona* spp., continuing a trend that started in the mid-2010s. Bottom dissolved oxygen saturation (O_2 sat) on the NL Shelf and the Grand Bank was higher than average in both years and, overall, higher in 2019 compared to 2020. Localized near-bottom aragonite undersaturation ($\Omega<1$) was observed on the Grand Bank and in the deeper slope waters off the Newfoundland Shelf, the Flemish Cap, and the tail of the Grand Bank in summer and/or fall for both years.

1. INTRODUCTION

The Atlantic Zone Monitoring Program (AZMP) was implemented in 1998 to enhance Fisheries and Oceans Canada's (DFO) capacity to describe, understand, and forecast the state of the marine ecosystem and to quantify the changes in the physical, chemical, and biological properties of the ocean (Therriault et al. 1998). A critical element of the AZMP involves the assessment of the fundamental relationships among the main components of the planktonic ecosystem to establish how they respond to changes in the marine environment.

Variability in biogeochemical oceanographic conditions is partly driven by the physical properties of the water masses. The southward flowing Labrador Current (LC) is the dominant feature that characterizes the oceanic circulation in the Newfoundland and Labrador (NL) Region. The inner branch of the LC brings cold and relatively low salinity waters flowing out of Baffin Bay and the Hudson Strait over the continental shelf (Wang et al. 2015; Florindo-López et al. 2020). The stronger outer branch carries warmer and more saline waters over the continental slope and rise into the Flemish Pass where it mixes with the warm and saltier waters of the North Atlantic Current (Krauss et al. 1990; Townsend et al. 2004) (Fig. 1A). A strong vertical density front at the shelf-break separates the cooler and fresher subarctic shelf waters from the warmer, more saline slope waters (Townsend et al. 2004). Another prominent feature of the NL shelf is the Cold Intermediate Layer (CIL), a cold water mass formed over the continental shelf during the spring when seasonal near-surface stratification isolate the cold winter mixed layer from the warmer atmosphere (Petrie et al. 1988; Cyr et al. 2011). The CIL is present during most of the year, maintaining bottom temperatures near or below 0°C on most of the shelf (see Cyr et al. 2021 for a detailed description of the physical marine environment).

The AZMP uses satellite remote sensing and *in situ* observations at a network of sampling stations distributed across four DFO Regions (Quebec, Gulf, Maritimes, and NL) to derive its information on the state of the marine ecosystem. In the NL Region, cross-shelf sections are sampled one to three times annually in the spring, summer, and fall during seasonal oceanographic surveys (Fig. 1B, C). In addition, one high-frequency coastal monitoring site "Station 27" located approximately four nautical miles off the entrance of St. John's Harbour is occupied opportunistically at a weekly to monthly rate between April and December with the highest number of occupations occurring in the spring and fall during DFO's multispecies surveys (Fig. 2). Oceanographic sections provide information about broad-scale environmental variability but with a temporal resolution limited to their seasonal coverage. The high-frequency monitoring site, on the other hand, allows for more detailed description of seasonal patterns. The location of the sampling stations and oceanographic sections occupied in 2019 and 2020 are presented in Figure 3.

A description of the spatial and temporal distribution of nutrients, phytoplankton, and zooplankton provides important information about the organisms at the base of the marine food webs and their relationship to the biogeochemical environment. Understanding the seasonal production cycles of plankton and their variability at annual to decadal time scales is essential to an ecosystem approach to fisheries management. This report provides an assessment of the biogeochemical oceanographic conditions in the shelf and slope waters of the NL Region in 2019 and 2020 in relation to long-term average conditions based on archived data and complements similar reviews of the physical and biogeochemical oceanographic conditions for the NL (Cyr et al. 2021), Gulf of St. Lawrence (Blais et al. 2021a, 2021b), and Scotian Shelf and Gulf of Maine (Casault et al. 2020, 2022) Regions as well as for the Northwest Atlantic shelf system as a whole (DFO 2020, 2021).

2. METHODS

To the extent possible, sample collection and processing conforms to established AZMP standard protocols described in Mitchell et al. (2002). Procedures for non-standard measurements or derived variables are described below. This report uses ecosystem production units (EPU), defined by the Northwest Atlantic Fisheries Organization (NAFO) to refer to the different subregions of the NL shelf and slope waters (Koen-Alonso et al. 2019); shown in Fig. 1C.

2.1. SATELLITE REMOTE SENSING OF OCEAN COLOUR

Near-surface Chl *a* concentrations, a proxy for phytoplankton biomass, were estimated from satellite ocean colour imagery collected by the Moderate Resolution Imaging Spectroradiometer (MODIS) Aqua sensor for different subregions spanning the NL shelf waters (Fig. 1C). Basic statistics (mean and standard deviation) were extracted from semi-monthly composite images to create visualization products of spatiotemporal variability in surface Chl *a* concentration.

We used the PhytoFit Shinny web application (Clay et al. 2021) to characterise the phenology of the spring phytoplankton bloom. PhytoFit allows users to view satellite Chl *a* and model phytoplankton blooms for regions with custom polygons. The three metrics used to characterize the spring phytoplankton bloom were: bloom initiation, bloom duration, and bloom magnitude.

These metrics were calculated for each year and subregion using a method adapted from Zhai et al. (2011). First, daily mean Chl *a* concentrations were derived from remote sensing reflectance using the POLY4 regional band-ratio algorithm (Clay et al. 2019). Then, for each year, a regression (span=0.2), weighed according to spatial percent coverage, was fitted to the annual time series of daily mean Chl *a* concentrations. Lastly, the fitted values of the loess regressions were used to model the spring bloom with a shifted Gaussian function of time from which the following bloom parameters were derived:

- **Bloom initiation** = day of year (DOY) when Chl *a* concentration increases to 20% of amplitude (i.e., max fitted value);
- **Bloom duration** = number of days separating the initiation and the end (DOY when Chl *a* concentration decreases to 20% of bloom amplitude);
- **Bloom magnitude** = area under the Gaussian curve.

The magnitude is an index of the spring phytoplankton biomass production. Only days comprised within the period extending from the winter low Chl *a* values to the lowest concentrations preceding the beginning of the fall bloom and for which satellite coverage of the subregion was ≥20% were used to model the spring bloom phenology.

2.2. SAMPLE COLLECTION

Seasonal oceanographic surveys were conducted along standard cross-shelf sections in the NL Region during 2019 (three surveys: spring, summer, fall) and 2020 (two surveys: summer, fall) in addition to occupations of Station 27 by ships of opportunity during multispecies surveys (Table 1, Fig. 1B). A total of 190 and 159 hydrographic station occupations were performed in 2019 and 2020, respectively (Table 1). Sampling consisted of vertical profiles of the water column carried out with a rosette-mounted CTD (SBE-9plus, Sea-Bird Electronics) fitted with dissolved oxygen (DO), fluorescence, photosynthetically active radiation (PAR), pH, coloured dissolved organic matter (CDOM), and transmissometer sensors. Water samples were collected in Niskin bottles at most stations at standard depths of 5, 10, 20, 30, 40, 50, 75, 100, 150, 250, 500, and 1,000 m and near the bottom depending on station bathymetry. All samples were

analyzed for nutrients (nitrate, silicate and phosphate) while Chl *a* concentration was measured up to a depth of 100 m along AZMP oceanographic sections, and across the entire water column (175 m) at Station 27. Total alkalinity (TA) and dissolved inorganic carbon (DIC) were also measured at a subset of stations and depths to monitor ocean acidification (OA). Zooplankton was collected by towing a conical ring net (75 cm diameter, 200 µm mesh) vertically at a speed of ~1 $m \cdot s^{-1}$ from near bottom (maximum depth of 1,000 m) to surface. Samples were preserved in a 2% buffered formaldehyde solution and analyzed for bulk biomass, abundance and diversity. Individuals were identified at a taxonomic rank deemed appropriate for the aim of the program with an emphasis on copepods with regards to taxonomic resolution (species or genus) and developmental stage (copepodite stages CI-CVI).

2.3. VERTICALLY INTEGRATED VARIABLES

Integrated Chl *a* (0–100 m) and shallow (0–50 m) and deep (50–150 m) nutrient inventories were calculated using trapezoidal numerical integration. Surface (0 m) values were taken as the closest near-surface measurement. When the maximum depth at a given station was shallower than the lower depth limit of the integration interval, the lower integration corresponds with the station depth. When not available, the value at the lower integration limit was taken as either

1. the interpolated value when sampling was deeper the lower integration limit, or
2. the closest deeper value when sampling was shallower than the lower integration limit.

2.4. ANNUAL ANOMALY SCORECARDS

Spatial and temporal trends of main biogeochemical indices are summarized in standardized anomaly scorecards. First, time series of vertically integrated nutrients, Chl *a*, and zooplankton inventories were modeled with a linear model of the form:

$$Density = \alpha + \beta_{YEAR} + \delta_{STATION} + \gamma_{SEASON} + \varepsilon$$

for the oceanographic sections where *Density* was in units of $mmol \cdot m^{-3}$ (nutrients), $mg \cdot m^{-3}$ (Chl *a*), $g \cdot m^{-2}$ (zooplankton biomass) or $individuals \cdot m^{-2}$ (zooplankton abundance), α is the intercept, ε is the error, and β, δ, and γ are the categorical effects of year, station, and season, respectively.

For the Station 27 time series, the model was :

$$Density = \alpha + \beta_{YEAR} + \delta_{MONTH} + \varepsilon$$

where β and δ are the categorical effects of year and month, respectively. For both models, data were natural log-transformed (ln) to normalize the skewed distribution of the observations. In the case of zooplankton, the number one (1) is added to the density before transformation (ln [*Density* + 1]) to include observations where density equals zero. The model's least square means based on type III sums of squares were used as estimates of annual means. For each index, annual anomalies were calculated as the deviation of an individual year from the long-term mean of the reference periods or climatology: 2003–20 for satellite ocean colour data, and 1999–2020 for nutrients, Chl *a*, and zooplankton inventories. Anomalies were expressed as standardized quantities, i.e., by dividing each anomaly by the standard deviation of the climatological mean.

2.5. DISSOLVED OXYGEN, PH AND CARBONATE CHEMISTRY

Results from DO analyses performed using the Winkler titration method (Winkler 1888) for all standard depths at a subsampled number of stations was used to calibrate the rosette-mounted DO sensor. Dissolved oxygen saturation (O_2 sat) in percentage (%) was calculated as the ratio

between the measured DO concentration and its solubility referenced to ocean surface using the TEOS-10 toolbox (McDougall and Barker 2011) and corresponding temperature-salinity (T-S) observations.

The pH (total scale) and aragonite saturation state (Ω_a) were calculated using the Python version (Humphreys et al. 2022) of the PyCO2SYS program (Lewis et al. 1998). The dissociation constants (K1, K2) of Mehrbach et al. (1973) refitted by Dickson and Millero (1987), total boron constant from Uppstrom (1974), and $KHSO_4$ constant from Dickson (1990) were used as recommended for best practices (Dickson et al. 2007; Chen et al. 2015; Orr et al. 2015).

3. OBSERVATIONS

3.1. SATELLITE OCEAN COLOUR

Satellite observations of ocean color provide a broad-scale perspective of the phytoplankton biomass in surface waters over the Northwest Atlantic. It is used here to supplement our ship-based observations and provide context for the interpretation of AZMP survey data. However, satellite observations do not inform on the vertical distribution of primary producers across the water column. Subsurface information is obtained through *in situ* sampling at Station 27 and along standard oceanographic sections during AZMP seasonal surveys.

3.1.1. Surface chlorophyll *a* concentration

Surface Chl *a* concentration in the NL Region is highest in the spring, lowest in summer, and intermediate in the fall. During the spring AZMP surveys, sea surface temperature (SST) is normally ≤0°C on the NL shelves and ranges between approximately 2–4°C on most of the Grand Bank and southern Newfoundland where the spring phytoplankton bloom is already well developed (Fig. 3). Sea ice cover along the coast of Labrador and northern Newfoundland in the spring limits satellite data availability for that area. During the summer surveys, SST on the Grand Bank and southern Newfoundland is typically >10°C and the spring phytoplankton bloom is mostly over. However, significant phytoplankton biomass is still present in early July in northern NL coastal waters and in the Labrador Sea where SST ranges between ~6-8°C (Fig. 3). During the fall surveys, SST has normally dropped below 0°C on the Labrador Shelf and varies between ~2–4°C on the Newfoundland Shelf, and between ~6–8°C on the Grand Bank and southern Newfoundland. Surface Chl *a* concentration is generally above the summer values across the Grand Bank and is highest in nearshore waters and in the south (Fig. 3). Reliable estimates of satellite-derived surface Chl *a* north of the 50°N are not available in the fall because of the limited daylight hours at the appropriate angle of incidence.

In 2019, Chl *a* concentration in the spring was higher than normal in southern Newfoundland, southern Grand Bank, and in the slope waters along the shelf break from northern Labrador to the tail of the Grand Bank (Fig. 4). In contrast, Chl *a* concentration was mostly near or below normal on the central and northern Grand Bank, the Newfoundland Shelf, and the Flemish Cap (FC; Fig. 4). Chl *a* concentration in summer was higher than normal on the northern Grand Bank and in the slope waters to the east, while negative anomalies were observed on most of the Labrador Shelf, off Newfoundland's Great Northern Peninsula, and in southern Newfoundland (Fig. 4). Data availability was limited in the fall but showed above-normal Chl *a* concentration on the FC area during the last two weeks of November (Fig. 4).

In 2020, surface Chl *a* concentration in the spring was higher than normal in Newfoundland Shelf slope waters (Fig. 5). Positive Chl *a* anomalies were also observed in the Labrador and Grand Bank slope waters as well as in Southern Newfoundland and on the southern Grand

Bank, while conditions were mostly near or below normal in shelf waters of central and northern Grand Bank (Fig. 5). During summer, Chl *a* was above normal on the northern Grand Bank and in northeast Newfoundland (St. Anthony Basin) as well as in the slope waters to the north, while negative anomalies were observed on most of the NL shelves and in the Labrador Sea (Fig. 5). Extensive cloud/fog cover over the Grand Bank and the FC during the first two weeks of July limited data availability for those regions. In the fall, Chl *a* levels were above normal across the northern Grand Bank and in southern Newfoundland, and near or above normal on the southern Grand Bank and in the slope waters to the east (Fig. 5).

3.1.2. Spring bloom phenology

We used daily surface Chl *a* concentrations from satellite imagery to estimate the initiation timing, duration and magnitude of the spring phytoplankton bloom within ten subregions spanning the NL Region from the Labrador Shelf to southern Newfoundland (Fig 1C). Bloom timing anomalies indicated periods of early and late blooms in 2005–06 and 2014–17, respectively, with no clear spatial or temporal trends in between except for the late blooms observed on the Flemish Cap/Pass and across the Grand Banks in 2003, and the notably earlier blooms on the Newfoundland Shelf, the Flemish Cap/Pass and the Grand Banks in 2010 (Fig. 6A).

Early bloom onsets are generally associated with longer bloom durations and vice versa (Fig. 6A, B). The magnitude of the spring bloom did not show clear spatial or temporal trends between 2003 and 2011 (Fig. 6C). Spring bloom magnitude remained mostly near or below normal from 2012 to 2017 before increasing to above-normal levels in recent years especially on the northern Grand Bank, in the Flemish Pass, and across most of the Newfoundland Shelf where record-high values were observed (Fig. 6C).

In 2019, the timing of the bloom was back to near normal almost everywhere except for the early blooms in the St. Anthony Basin and on the St. Pierre Bank, and for the late bloom in the northeast Newfoundland waters (Fig. 6A). Blooms were shorter than normal in northeast Newfoundland waters and on the Flemish Cap/Pass, and longer than normal on the Grand Bank, St. Pierre Bank, and in the St. Anthony Basin where the longest bloom since 2003 was recorded for that subregion (Fig. 6B). Bloom magnitude continued to be higher than normal on the northern Grand Bank, in the Flemish Pass, and on most of the Newfoundland Shelf with a record-high value for the northeast Newfoundland subregion (Fig. 6C). Spring bloom magnitude reached a record low value on the Hamilton Bank, was below normal on the FC, and near normal elsewhere (Fig. 6C).

In 2020, spring bloom initiation was near normal on the FC and the Grand Banks with the exception of the Southeast Shoal where the bloom was slightly late (Fig. 6A). Blooms were earlier than normal on most of the Newfoundland Shelf and central Labrador, and later than normal in northern Labrador (Fig. 6A). Bloom duration was shorter than normal across the region except for the slightly longer blooms on the Hamilton Bank and the northeast Newfoundland subregions (Fig. 6B). Record-low durations were observed for the northern Labrador and St. Anthony Basin subregions (Fig. 6B). Spring bloom magnitude was at a record-high on the Hamilton Bank and above normal on the Southeast Shoal and St. Pierre Bank, and near-to-below normal elsewhere (Fig. 6C).

3.2. NUTRIENTS AND CHLOROPHYLL *A* INVENTORIES

Nitrate, silicate, and phosphate concentrations generally show similar seasonal patterns characterized by strong vertical gradients throughout most of the year. Nutrient concentrations are typically lower in the upper water column where photosynthesis, fueled by nutrients and

light, occurs at a higher rate than at greater depths. In the Northwest Atlantic, the concentration of nutrients in the upper water column is highest during the winter when low surface water temperature and wind favor vertical mixing (Figs. 7, 8, and 9). In the spring, the onset of water column stratification and the increasing daylength trigger the initiation of the spring phytoplankton bloom. Increasing rate of nutrients uptake by rapidly developing phytoplankton biomass in surface waters leads to the development of a nutricline (i.e., a strong vertical gradient in nutrient concentration characterized by depleted nutrient levels in surface waters) which persists throughout the summer. In the fall, the weakening of the water column stratification allows for the replenishment of surface nutrient stocks through the vertical mixing of deeper nutrient-rich waters with surface waters (Figs. 7, 8 and 9).

3.2.1. Station 27

Nutrient climatologies at Station 27 show that important drawdowns normally occur in April in the top 100 m of the water column for nitrate and silicate, and top 50 m for phosphate. Surface nutrient concentrations then remain low throughout the summer until they start rising again in October-November (Figs. 7A, 8A and 9A). Nitrate gets nearly depleted by June in surface waters, which typically marks the end of the spring bloom (Figs. 7A and 10A). Slight increases in surface nitrate and silicate are normally observed in August before surface concentrations decline again in September and October during the fall bloom (Figs. 7A, 8A and 10A). Phosphate is typically minimum in surface waters from June through September without however getting entirely depleted (Fig. 9A). There is less variability in the deeper water nutrient inventories. Bottom concentrations are generally lowest in February and March when the water column is well mixed. Concentrations then gradually increase throughout summer and fall as organic matter produced in surface waters sinks and accumulate at the bottom where it gets re-mineralized by microbial activity (Figs. 7A, 8A and 9A).

Chl *a* concentration at Station 27 normally increases rapidly in March, reaches a maximum in April, and declines afterward until the end of the spring bloom in June (Fig. 10A). Most of the phytoplankton production in the spring occurs in the top 100 m of the water column, which also corresponds to the nutricline depth for nitrate and silicate. Limited nutrient drawdowns at depths >100 m suggests that downward transport of phytoplankton cells produced in the upper water column during the spring bloom is mainly responsible for the higher Chl *a* concentrations in deeper waters during that time of the year (Figs. 7A, 8A and 10A). A second period of phytoplankton proliferation generally occurs between August and October. This fall bloom is less intense than the spring one and is limited to the upper water column as the water column is still considerably stratified (Fig. 10A).

In 2019, the spring bloom was particularly intense at Station 27 with peak Chl *a* concentrations in surface waters up to two times higher than the climatological means (Fig. 10B). Important nutrient drawdowns observed throughout the water column in May suggested that phytoplankton growth occurred at greater depths than usual (Figs. 7B, 8B and 9B). The fall bloom was also more intense than normal but its timing, duration and vertical extent were comparable to the climatology (Fig. 10A). Nitrates in the top 40 m of the water column were almost entirely depleted from May through October (Fig. 7B). Important silicate drawdown occurred at depths of up to 150 m in May with low levels persisting until August in the top 80 m (Fig. 8B). Phosphate reached its minimum surface concentration during the fall bloom with significant drawdowns at depths up to 60 m, so approximately two times deeper than normal (Fig. 9B). Bottom concentrations of nitrate and silicate were higher than normal in summer and fall (Figs. 7B and 8B) while those of phosphate were above normal during summer and below normal in the fall (Fig. 9B).

No data were collected at Station 27 before July in 2020, thus preventing the monitoring of the spring bloom. The fall bloom was earlier and more intense than usual with high subsurface Chl *a* concentrations in July and September (Fig. 10C). Transient intrusions of nitrate and phosphate in surface waters in October suggested wind-induced mixing in the top layer of the water column in early fall (Figs. 7C and 9C). Bottom nutrient concentrations in the fall, especially for nitrate and phosphate, were above the long-term seasonal means (Figs. 7C, 8C and 9C).

3.2.2. Oceanographic sections

Annual anomaly time series of shallow (0–50 m) and deep (50–150 m) inventories of nitrate, silicate, and phosphate along standard AZMP oceanographic sections and at Station 27 are used to assess long-term spatial and temporal trends in the NL Region. Variability in nutrient inventories is generally higher in the upper water column where most of the phytoplankton growth and associated nutrient uptake occurs. Deep-nutrient inventories are less affected by the growth of phytoplankton and are therefore better indicators of nutrient standing stocks potentially available to primary producers. Nonetheless, shallow- and deep-nutrient inventories showed overall coherent spatial and temporal trends over the past two decades except for the contrasting anomaly patterns during the early years of the program (Figs. 11 and 12).

Integrated shallow nitrate and silicate inventories were mostly above normal during the early and mid-2000s, and variable but mostly near or below normal after 2007 with the exception of several positive nitrate anomalies during the 2015–17 period, including a record-high value on the southeastern Grand Bank (SEGB) in 2017 (Fig. 11A, B). Shallow phosphate inventories also transitioned from mainly near-to-above-normal levels between 1999 and 2011, to mainly near-to-below normal throughout the 2010s with mainly positive anomalies in 2015 and 2016 (Fig. 11C).

In 2019 and 2020, shallow nitrate inventories were mainly below normal except for the positive anomalies observed on Seal Island (SI) in 2019, and at Station 27 in 2020 (Fig. 11A). Silicate inventories were near or below normal in 2019, and respectively near and above normal on the Newfoundland Shelf and the Grand Bank in 2020 (Fig. 11B). Shallow phosphate inventories were mainly below normal in 2019 and 2020, continuing a trend that started in 2017 (Fig. 11C).

Deep nutrient inventories also showed overall decreasing trends over the time series (Fig. 12A–C). Both nitrate and silicate inventories transitioned from mainly above normal to mainly below normal around 2010 and 2011, respectively (Fig. 12A, B). Deep phosphate inventories declined from above normal in the early 2000s when record-high anomalies were recorded on each oceanographic section and at Station 27, to near normal from the mid-2000s until the early 2010s, and to mainly below normal afterwards (Fig. 12C). The lower climatological means for the deep nutrient inventories on SEGB are driven by the shallower station depths on that section which, in most cases, are considerably less than the lower integration boundary of 150 m (Fig. 12A–C).

Deep nitrate and silicate inventories showed similar spatial patterns in 2019 with below-normal levels at Station 27, near-normal levels on SEGB, and above-normal levels on the Newfoundland Shelf (Bonavista Bay [BB] and SI) and the northern Grand Bank (FC section), including a record-high value for nitrate on SI (Fig. 12A, B). In 2020, deep nitrate and silicate inventories were mainly near normal, and above normal, respectively. Deep phosphate inventories were near normal on all oceanographic sections in 2019 and 2020, but respectively below and above normal in 2019 and 2020 at Station 27 (Fig. 12C).

There was an overall decrease in Chl *a* inventories from 1999 until the mid-2010s with integrated concentrations transitioning from mainly above normal from 1999 to 2001, to near normal from 2002 to 2010, and to below normal from 2011 to 2016 (Fig. 13). Chl *a* inventories

then increased to mainly above normal from 2017 to 2019 with the exception of the low levels recorded on SEGB in 2017 and on FC in 2019. In 2020, Chl *a* inventories were back to near normal except on SI where Chl *a* concentration remained above normal for a fourth consecutive year (Fig. 13).

Chl *a* inventories were not related to shallow nutrients or to deep silicate and phosphate inventories but was positively related ($p<0.001$) to one year lag nitrate inventories (Fig. 14), thus supporting the use of deep nitrate inventories as indicators of the phytoplankton production potential at the regional scale. In general, trends in both shallow and deep nutrient as well as Chl *a* inventories were consistent between the Grand Bank and the Newfoundland Shelf suggesting that nutrient inventories in coastal NL waters are regulated by broad-scale oceanic circulation across the region.

3.3. ZOOPLANKTON

3.3.1. Station 27

3.3.1.2. Community composition

The abundance and biomass of mesozooplankton in the North Atlantic is typically dominated by copepods. At Station 27, copepods normally account for ≥80% of total zooplankton abundance with their relative abundance being lowest in spring and highest in winter (Fig. 15A). The vast majority of copepods at Station 27 can be grouped into 11 species or genera, whose proportion vary seasonally (Fig. 15B). Small *Oithona* spp. copepods are the most abundant year round, followed by *Pseudocalanus* spp. (Fig. 15B). The large, energy-rich *Calanus finmarchicus* are also well represented from June to November while the proportion of small *Temora longicornis* becomes significant from August to December (Fig. 15B). *Calanus glacialis* and *Calanus hyperboreus* are among the largest copepods in the Northwest Atlantic. Their abundance at Station 27 is normally highest from May to July (Fig. 15B). The remaining taxa are generally present year round, but in proportions rarely exceeding 5% of the total copepod abundance (Fig. 15B).

The non-copepod zooplankton community at Station 27 is dominated by appendicularians (e.g., *Frittilaria* spp., *Oikopleura* spp.), pteropods (e.g., *Limacina helicina, Limacina retroversa*), bivalve larvae, and cladocerans (Fig. 15C). The proportion of appendicularians peaks from May to July, while that of pteropods remains high from September to April (Fig. 15C). Bivalve larvae are present year round in the water column, accounting for up to 20% of the non-copepod community from August through January (Fig. 15C). Cladocerans are present in smaller proportions in spring and fall but generally become more abundant during the summer months (Fig. 15C). Chaetognaths, malascostraceans (mainly hyperiid amphipods, euphausiids, shrimps, and mysids), and cnidarians/ctenophores are present at Station 27 during most of the year but in proportions generally not exceeding 5% of total non-copepod abundance (Fig. 15C). The "others" category contains larval and juvenile fish as well as larval stages of other invertebrates including polychaetes, echinoderms and bryozoans (Fig. 15C).

In 2019, the proportion of non-copepod zooplankton was up to two times higher than average in the spring, and about 20% lower than average in the fall (Fig. 15D). The main differences in copepod community composition and seasonality between 2019 and the climatology included the higher proportion (~3x) of *C. hyberboreus* in spring and summer, the one month delay in the emergence of *T. longicornis* in the fall, and the higher proportion of *Oithona* spp. in November and December (Fig. 15E). The proportion of *C. finmarchicus* was two times higher than average in August 2019, but about 50% lower than the climatological mean from September through December (Fig. 15E). The community of non-copepods showed important deviations from the

climatology in 2019. The proportion of appendicularians was 15–40% higher than average in spring and summer, while that of pteropods was down by 20% in April, and up by 30% in September (Fig. 15F). Cladocerans, which normally account for 5–20% of non-copepods in summer and fall, were nearly absent in 2019 (Fig. 15F).

In 2020, the relative abundance of copepods and non-copepods was similar to the climatology from July through December (Fig. 15G). The proportion of *Oithona* spp. copepods was 15–25% higher than average from September to November, while that of *Pseudocalanus* spp. was about 30% lower than average in October, and 25–45% higher from November through December (Fig. 15H). The proportion of *T. longicornis* remained relatively low in late summer and peaked at about 20% in October (Fig. 16H). Similarly to 2019, the proportion of *C. finmarchicus* was on average approximately 50% lower than the climatology in the fall (Fig. 15H). The community of non-copepods in 2020 mostly deviated from the climatology owing to a higher proportion of pteropods in the fall, and a 40% decrease in appendicularians from October through December (Fig. 15I).

3.3.1.3. Zooplankton abundance and biomass

Total abundance of copepods at Station 27 is typically lowest in the spring and increases throughout summer to a maximum in September. Copepod abundance generally remains somewhat stable during the fall and starts to decline in February (Fig. 16A). The abundance of non-copepod zooplankton generally increases throughout spring and summer with a slight drop in June, peaks in September, and declines in the fall to a minimum during the winter months (Fig. 16B).

The total zooplankton biomass at Station 27 starts to increase at the end of the winter and reaches a maximum value in April followed by a second, more modest peak in June (Fig. 16C). The biomass then declines throughout the summer to a minimum in August before stabilizing at slightly higher levels during the fall (Fig. 16C). It is worth mentioning that, although plankton tows target mesozooplankton (i.e., ≥200 µm mesh), colonial forms of phytoplankton may also be retained in the net. This is especially true in the spring when large chain-forming diatoms dominating the assemblage inflate biomass and contribute to the peak observed in April.

In 2019, total copepod abundance was below or near normal during the spring, near normal in summer, and mostly above normal in the fall (Fig. 16A). The abundance of non-copepod zooplankton was near normal in the spring, and near or above normal during summer and fall (Fig. 16B). Total zooplankton biomass was below normal in the spring, and mainly above normal during summer and early fall but returned to near-normal levels in November and December with the high December biomass value driven by above-normal abundances of both copepods and non-copepods (Fig. 16C).

In 2020, the abundance of copepods was mainly above normal in summer and near normal in the fall with the exception of one markedly high abundance value in mid-December (Fig. 16A). Total non-copepod abundance was mainly near normal in summer and above normal in the fall with a few high values in November and December (Fig. 16B). Zooplankton biomass was below or near normal in summer and early fall, and near normal in November with a particularly high value recorded in early December (Fig. 16C).

3.3.1.4. Dominant species and population dynamics

The large calanoid copepods *C. finmarchicus*, *C. glacialis*, and *C. hyperboreus* display similar seasonal patterns with abundance increasing in the spring to a maximum in early summer (Fig. 17A–C). The abundance of *C. finmarchicus*, however, gradually decreases throughout summer, fall and winter while that of *C. glacialis* and *C. hyperboreus* rapidly declines after peaking in June and July, respectively (Fig. 17A–C). *C. finmarchicus* is the most abundant with

a mean maximum abundance approximately 1.5 and five times higher than that of *C. glacialis* and *C. hyperboreus*, respectively (Fig. 17A–C).

Seasonal abundance patterns of small copepods at Station 27 contrast with those of the large calanoids. The abundance of *Oithona* spp. is typically lowest in late spring and gradually increases throughout summer and fall to peak in December and January (Fig. 17D). The abundance of the small calanoids *Pseudocalanus* spp. and *Temora longicornis* is generally lowest in spring, increases during summer to a maximum in September, and gradually declines during the fall and winter (Fig. 17E, F). Contrary to *Oithona* and *Pseudocalanus*, which numerically dominate the copepod community year round, *T. longicornis* occurs in low abundance from February through June at Station 27 (Figs. 15B and 17F).

In 2019, spring abundance of the three large calanoid species was mostly below or near normal with the exception of a few above-normal values in April and May (Fig. 17A–C). The abundance was more variable in summer with some above- and below-normal values between June and August, but was mainly above normal for *C. hyperboreus* (Fig. 17A–C). Fall abundances were near or below normal for *C. finmarchicus* and near normal for *C. glacialis* and *C. hyperboreus* (Fig. 17A–C). The abundance the small *Oithona* spp. and *Pseudocalanus* spp. copepods was below or near normal in the spring and summer, and mostly above normal during the fall with several values two to three times higher than the climatological mean from September to November (Fig. 17D, E). As expected, the abundance of *T. longicornis* was low during spring but, similarly to the other two small copepods, its abundance was markedly higher than normal in September and October (Fig. 17F).

In 2020, the abundance of *C. finmarchicus* was mostly below normal from August to December while that of *C. glacialis* and *C. hyperboreus* was near normal during the same period (Fig. 17A–C). For the small copepods, the abundance of *Oithona* spp. and *Pseudocalanus* spp. was mostly above normal in late summer and near normal in the fall with the exception of high *Pseudocalanus* values in late November and December (Fig. 17D, E). The abundance of *T. longicornis* was mostly below or near normal from August to December despite a few markedly high values in October and December (Fig. 17F).

Copepods are an important food source for several larval, juvenile and adult fish. Because of their abundance and high energetic value, *C. finmarchicus* and *Pseudocalanus* spp. are often preferentially selected by fish targeting specific copepodite stages (CI-CVI) best suited for their size and mouth gape. The proportion of adults (CVI) *C. finmarchicus* at Station 27 normally increases in January and peaks in April at about 50% before declining rapidly as the new generation develops (Fig. 18A). Young CI-CIV copepodite stages make up 75–90% of the population from May through August while subadults (CV) account for 40–50% from September to December (Fig. 18A).

The population structure of *Pseudocalanus* spp. is similar to that of *C. finmarchicus* with the proportion of adults peaking at ~50% in April and young CI-CIV stages making up 55–75% of the population from May through August (Fig. 18B) but with CI-CIV stages generally peaking in August compared to July such as in the case of *C. finmarchicus*. The fall population is also more evenly distributed among CIII (~20%), CIV (~30%), and CV (~25%) stages from September through December (Fig. 18B). Despite clear seasonal patterns in the population structure, all stages of both taxa are present year round at Station 27.

In 2019, the seasonal pattern in *C. finmarchicus* population structure was similar to the climatology from April to December despite a certain delay in the production cycle of young copepodite stages. The proportion of CI-CIV stages in May was 15% less than average and CI and CII stages peaked in June, so approximately one month later than usual (Fig. 18C). For *Pseudocalanus* spp., the proportion of CI-CII stages was 30% higher than average from May

through July, but the population structure was similar to the climatology during the rest of the year (Fig. 18D).

In 2020, the proportion of *C. finmarchicus* that had matured into CV subadults in the fall (October-December) was ~30% higher than usual (Fig. 18E). The population structure of *Pseudocalanus* spp. did not depart much from the long-term average during the July-December period for which data were available (Fig. 18F).

3.3.2. Oceanographic sections

3.3.2.1. Zooplankton abundance and biomass

Annual anomaly scorecards showed that the abundance of copepod and non-copepod zooplankton was minimum during the late 1990s and early 2000s when several record-low values were recorded (Fig. 19A, B). On the Grand Bank, zooplankton abundance gradually increased since 1999 with anomalies transitioning from mostly negative to mostly positive around 2010 (Fig. 19A, B). Zooplankton abundance was more variable on the Newfoundland Shelf where periods of low and high abundances alternated throughout the time series (Fig. 19A, B). The abundance of both copepods and non-copepods have remained mostly above normal across the NL Region since the mid-2010s (Fig. 19A, B).

Total zooplankton biomass was at minimum in the early years of the program along the oceanographic sections, but mainly above normal at Station 27 during the same period (Fig. 19C). Zooplankton biomass increased to mainly near- or above-normal levels from 2002 to 2011 before declining to near-to-below-normal levels from 2012 to 2015 (Fig. 19C). Zooplankton biomass has remained mainly near or above normal across the Region since 2016 (Fig. 19C).

In 2019, copepods showed the same abundance pattern as during the previous year with near-normal abundances on the Newfoundland Shelf (SI and BB) and on FC, and above-normal abundances on SEGB and at Station 27 (Fig. 19A). The abundance of non-copepod zooplankton decreased compared to the previous year, but remained mainly above normal across the region (Fig. 19B). Zooplankton biomass also decreased compared to the previous year and was near normal except on SEGB where biomass reached its second lowest value of the time series (Fig. 19C).

In 2020, copepod abundance was above normal across most of the region with record-high values on the Newfoundland Shelf (SI and BB) and at Station 27 where abundance has remained above normal for seven consecutive years (Fig. 19A). The abundance pattern for non-copepods was similar to that of copepods with above-normal levels everywhere except for FC and, a record-high value on SI (Fig. 19B). Zooplankton biomass was near normal on the Grand Bank (FC and SEGB) but increased to above normal on the Newfoundland Shelf (SI and BB; Fig. 19C).

3.3.2.2. Dominant copepod taxa

The abundance of the three *Calanus* species varied similarly in space and time since 1999. Abundances were generally near or above normal throughout the 2000s and peaked around 2009–11 for *C. glacialis* and *C. hyperboreus* (Fig. 20A–C). The abundance of the three *Calanus* species decreased to mainly near- or below-normal levels during the early and mid-2010s and were variable but mainly near normal during the second half of the 2010s (Fig. 20A–C).

In 2019, the abundance of *C. finmarchicus* and *C. glacialis* was variable across the Region without departing too much from normal levels except for the stronger negative Station 27 and positive (BB) *C. glacialis* anomalies at Station 27 (Fig. 20A, B). The abundance of

C. hyperboreus was mainly near or below normal, continuing a trend that started in 2016 (Fig. 20C).

In 2020, the abundance of *C. finmarchicus* was below normal across the Grand Bank, near normal on BB, and above normal on SI with record-high and record-low values on SI and FC, respectively (Fig. 20A). The abundance of *C. glacialis* and *C. hyperboreus* was near- or above-normal except for the negative *C. glacialis* anomaly observed on FC (Fig. 20C, D).

The abundance of small calanoid (*Pseudocalanus* spp., *T. longicornis*) and cyclopoid (*Oithona* spp.) copepods gradually increased throughout the time series on the Grand Bank with anomalies transitioning from mostly negative to mostly positive around 2009 for *Oithona* and *Pseudocalanus,* and around 2011 for *T. longicornis* (Fig. 21A–C). Abundance patterns were more variable on the Newfoundland Shelf where above-normal levels were observed from 2003 to 2010, especially for *Pseudocalanus* and *Oithona* (Fig. 21A, B). The abundance of all three small copepod taxa has remained mainly above normal in the NL Region since the mid-2010s except for SI where the abundance of *T. longicornis* has remained below normal since 2017 (Fig. 21A–C).

In 2019, the abundance of *Pseudocalanus* spp. was near normal across the Region except for SEGB where abundance was slightly above normal (Fig. 21A). The abundance of *Oithona* spp. was above normal at Station 27 and on SEGB, and near normal elsewhere, while that of *T. longicornis* was near normal on the Grand Bank and below normal on the Newfoundland Shelf (Fig. 21B, C).

In 2020, the abundance of *Pseudocalanus* spp. and *Oithona* spp. was above normal on the Newfoundland Shelf and at Station 27 with record-high values on SI for *Oithona,* and on BB and at Station 27 for both species (Fig. 21A, B). The abundance of *T. longicornis* was above normal on BB and at Station 27, near normal on FC, and below normal on SEGB and SI (Fig. 21C).

3.3.2.3. Non-copepod zooplankton

The community of non-copepod mesozooplankton in the NL Region is numerically dominated by appendicularians, pteropods, and bivalve larvae. The abundance of appendicularians and pteropods was more variable on the Newfoundland Shelf compared to the Grand Bank where anomalies went from mostly negative to mostly positive around 2010 (Fig. 22A, B). The abundance of bivalve larvae showed less spatial variability. It was highest in the late 1990s and early 2000s and declined below the long-term average across the Region throughout most of the 2000s before increasing again in the early 2010s to near- or above-normal levels where it has since remained (Fig. 22C).

In 2019, the abundance of appendicularians and bivalve larvae was near or above normal across the Region with a record-high value for bivalve larvae on SI (Fig. 22A, C). The abundance of pteropods above normal on SEGB for a fourth consecutive year and near normal elsewhere (Fig. 22B).

In 2020, the abundance of appendicularians was above normal on the Newfoundland Shelf but decreased to near normal on the Grand Bank after eight years of mostly above-normal levels (Fig. 22A). The abundance of pteropods increased from near normal to above normal on the Newfoundland Shelf and at Station 27 with record-high values on SI and at Station 27, but remained near normal on FC for a third consecutive year and above normal on SEGB for a fifth consecutive year (Fig. 22B). The abundance of bivalve larvae was near normal everywhere except for the slightly above-normal level recorded on BB (Fig. 22C).

3.4. DISSOLVED OXYGEN

O_2 sat ranged between 60% and 100% in near-bottom waters of the Newfoundland Shelf and the Grand Bank, with generally higher saturation levels in 2019 compared to 2020, and in summer compared to fall (Fig. 23). In 2019, O_2 sat was above the 2014–20 mean on the Newfoundland Shelf (SI section), the norther Grand Bank and the Flemish Cap (FC section), with saturation levels >95% across the water column on SI (Fig. 24) and >80% on the FC (Fig. 25).

O_2 sat levels in 2020 deviated less from the 2014–20 mean conditions compared to the previous year. Saturation was mostly above average in SI surface waters with a few pockets of lower-than-average levels near the bottom in the shallower portions of the shelf (Fig. 24). On the FC section, O_2 sat was especially high in nearshore waters and around the Flemish Cap with a few pockets of lower-than-average levels at intermediate depths (Fig. 25).

3.5. OCEAN ACIDIFICATION

Many marine organisms produce skeletons and shells made of aragonite — a specific form of calcium carbonate ($CaCO_3$). The saturation state of aragonite (Ω_a) is a measure of how easily aragonite can dissolve in seawater. The lower the saturation level, the more difficult it is for organisms to build and maintain their protective skeletons and shells. When $\Omega_a>1$, seawater is supersaturated with $CaCO_3$ and conditions are favorable for shell and skeleton formation. At $\Omega<1$, seawater is undersaturated with $CaCO_3$ and conditions become corrosive for aragonite-based shells and skeletons.

During summer 2019, bottom conditions were supersaturated with regards to aragonite on the Newfoundland Shelf (MB, SI, and BB) but mostly undersaturated on the northern Grand Bank (Station 27 and inner portion of FC; Fig. 26). In the fall, bottom conditions were supersaturated almost everywhere on the Newfoundland Shelf, over the FC, and in southern Newfoundland but Ω_a values were close to one on most of the Grand Bank and in deeper slope waters east to the FC (Fig. 26).

On SI, summer pH ranged between 8.1 and 8.2 in surface waters and below 200 m in the slope waters and between 8.0 and 8.1 below the surface and down to the bottom on the shelf portion of the section (Fig. 27). The entire water column was supersaturated with $CaCO_3$ ($\Omega_a>1$) in summer, although small pockets of near-saturation levels were present on the shelf at intermediate depths (Fig. 28). For both metrics, this generally corresponded to conditions below the 2014–20 average at intermediate depths inshore and on the outer shelf, and above-average conditions in surface and near-bottom waters on the inner and outer portion of the shelf as well as across the water column on the middle portion of the shelf and in slope waters (Figs. 27 and 28).

On FC, summer pH ranged mostly between 8.0 and 8.1 with a subsurface layer of higher (8.1–8.2) pH, and more acidic conditions (pH 7.8–8.0) near the bottom on the inner and outer portions of the shelf and on the FC (Fig. 29). Conditions were undersaturated with $CaCO_3$ near the bottom on the deeper portions of the inner shelf with Ω_a values ranging from 0.8–1.0 (Fig. 30). For both metrics, this corresponded to above-average conditions for the surface and intermediate depths on the shelf and across the water column in the Flemish Pass and off the FC to the east, and to below-average conditions near the bottom for the inner shelf and above of the FC (Figs. 29 and 30).

In 2020, bottom pH was generally higher on the Newfoundland Shelf (MB, SI, and BB) compared to the Grand Bank (Station 27, FC, and SEGB) and, although pH did not vary seasonally on BB, conditions on the northern Grand Bank (FC) were more acidic in summer

compared to fall (Fig. 26). Bottom conditions were undersaturated with $CaCO_3$ on various portions of the Grand Bank in both summer and fall, but also in the deeper slope waters off the FC and the southern Grand Bank in the fall (Fig. 26).

On SI, summer pH decreased with increasing depth and ranged between 8.1 and 8.2 in surface waters, between 8.0 and 8.1 at intermediate depths and near the bottom on the shelf, and between 7.9 and 8.0 in the deeper waters of the shelf break (Fig. 27). These values were generally below the long-term average for the surface waters over the shelf and near the bottom on the outer shelf and in subsurface slope waters down to 500 m, and above average at intermediate depths and near the bottom on the inner shelf and in surface slope waters (Fig. 27). Conditions were supersaturated with $CaCO_3$ across the water column with Ω_a values between 1.2 and 2.4 and decreasing with depth at higher rate on the shelf compared to slope waters (Fig. 28). These values were mainly above average for surface and bottom shelf waters and across the entire water column for the inner and outer shelf, and below average at intermediate depths on the middle portion of the shelf and in subsurface waters down to 500 m on the continental slope (Fig. 28).

On the FC section, summer pH ranged mostly between 8.0 and 8.1 in surface waters and at intermediate depths, and between 7.9 and 8.0 near the bottom on the shelf and in subsurface waters around the Flemish Cap (Fig. 29). Slightly more acidic (pH 7.8–7.9) conditions were present on the shallower portion of the shelf (Fig. 29). Conditions were mostly supersaturated with $CaCO_3$ with Ω_a ranging between 1.4 and 2.2 in surface waters, and between 1.0 and 1.2 at intermediate depths and near the bottom with the exception of a few slightly undersaturated bottom locations in shallower shelf regions (Fig. 30). For both metrics, this corresponded to mostly above-average conditions for surface and near-bottom waters on the shelf, and to below-average conditions at mid-water depths on the shelf and in subsurface waters down to 500 m in the Flemish Pass and around the FC (Figs. 29 and 30).

4. DISCUSSION

4.1. NUTRIENTS AND CHLOROPHYLL

Phytoplankton production occurs in the euphotic zone — the uppermost, well-lit layer of the ocean — and is chiefly controlled by irradiance and nutrient availability. In Northwest Atlantic coastal waters, the euphotic depth is generally <80 m (Casault et al. 2022; Maillet et al. 2022). Nitrogen is the main limiting factor of phytoplankton growth in the ocean but phosphorous may also become limiting, especially in the fall (Howarth 1988). Phytoplankton assemblages are generally dominated by diatoms — large phytoplankton cells enclosed in siliceous capsules — during the spring and the fall when nitrate concentrations are high, and by smaller flagellates and dinoflagellates in the summer when nitrate concentrations are low (Horwood et al. 1982; Dauchez et al. 1996; Casault et al. 2022). Vertical profiles of nutrients and Chl *a* at Station 27 show that nitrate depletion generally marks the end of the spring bloom. However, in years of intense production like in 2019, silicate may also limit the diatom-driven spring production (Krause et al. 2019).

Nutrient inventories in surface waters are affected by primary production processes and are therefore more variable in shallower compared to deeper water. Additionally, annual variability in physical drivers such as sea temperature, salinity, light, and sea ice affect the timing and intensity of spring and the fall blooms (Townsend et al. 1994; Wu et al. 2007). Each AZMP seasonal survey covers large areas of the NL Shelf over a period of ~3 weeks. Consequently, the synchronicity of the survey timing relative to primary production cycle affects *in situ* measurements and partly explains the absence of relationships between anomalies in surface

nutrient and Chl-*a* inventories. Deep nutrient inventories are, however, more representative of the biogeochemical characteristics of prevalent water masses in the area (Joyce et al. 2001). The significant relationship ($p<0.001$) between one year lagged nitrate and Chl *a* anomalies highlight the relationship between deep-water nutrients inventories and phytoplankton production at the regional scale and the critical role of nitrate in controlling ocean primary production.

In temperate seas, the spring phytoplankton bloom is a critical event with important implications on overall ecosystem productivity. The timing, duration and magnitude of the spring bloom directly or indirectly impacts reproduction, growth and recruitment of several species including zooplankton (Head et al. 2000), fish (Cushing 1990; Kristiansen et al. 2011; Buren et al. 2014; Mullowney et al. 2016), seabirds (Durant et al. 2003; Regular et al. 2014), and marine mammals (Hlista et al. 2009). Spring bloom phenology indices derived from satellite observations showed a general shift toward earlier onsets of spring blooms across most of the NL Region in 2019 and 2020 compared to the 2014–18 period. The higher-than-normal silicate inventories (50–150 m) observed across most of the Newfoundland Shelf and the Grand Bank in 2019 and 2020 may have favoured the faster development of the large diatoms cells that dominate the spring phytoplankton assemblages.

The SI section is not sampled in the spring and, consequently, the biogeochemical indices for the *in situ* observations including Chl *a* biomass index, are calculated using summer and fall data only. A moderate spring phytoplankton biomass is not necessarily incompatible with proportionally high summer and/or fall production. This could partly explain the contrast between the high Chl *a* biomass index for SI and the low spring bloom magnitude for the geographically corresponding Hamilton Bank subarea in 2019. On the other hand, the BB and FC sections are generally sampled the spring, summer, and fall and the climatologies used in the anomaly calculation for these sections include data from all seasons. Phytoplankton biomass in the water is highest during the spring bloom (Dauchez et al. 1996; Craig et al. 2015) and, although the linear model used to derive Chl *a* biomass estimates includes a season effect, missing data from spring surveys is likely to produce lower annual mean values. Consequently, the near-normal Chl *a* inventories for BB in 2019 and 2020, and for FC in 2020 likely underestimate the true annual phytoplankton production but it is unclear to what extent. The same can be said about the above-normal (2019) and near-normal (2020) Chl *a* inventories for the SEGB section where annual estimates and climatologies are generally based on spring and fall data and where no spring surveys occurred in both years.

4.2. ZOOPLANKTON ABUNDANCE, BIOMASS AND COMMUNITY COMPOSITION

Zooplankton abundance and biomass indices indicate a change in the size structure of the community toward smaller individuals that occurred between the early 2000s and the mid-2010s. This was particularly apparent on the Grand Bank where the increase in abundance was more consistent and where abundance anomalies shifted from mostly negative to mostly positive around 2010, while total zooplankton biomass transitioned from above to below normal during the same period. The increase in copepod abundance on the Grand Bank was mainly driven by the small copepod taxa *Pseudocalanus* spp. and *Oithona* spp. which numerically dominate the mesozooplankton assemblage year round, but also by *Temora longicornis* that normally becomes abundant in the fall (Pepin et al. 2011). Contrary to the small taxa, the abundance of the large calanoid copepods *C. finmarchicus*, *C. glacialis*, and *C. hyperboreus* decreased during the early to mid-2010s. The abundance of large calanoids is considerably less compared to that of the small taxa and their decline had limited impact on the overall increasing abundance trend. However, their abundance decline was directly responsible for the decrease in total zooplankton biomass observed during that period given that large calanoids, and

especially *C. finmarchicus*, generally account for more than half of the total zooplankton biomass in the North Atlantic (Planque and Batten 2000; Head et al. 2003).

Long-term abundance patterns of copepods were more variable on the Newfoundland Shelf with high abundances during the 2000s driven by above-normal levels of small taxa. In 2019 and 2020, copepod abundance was at record-high levels on both SI and BB. The missing spring survey on BB in 2020 may have slightly inflated the abundance estimate for that year since copepod abundance generally peaks in summer and fall. The missing spring survey in 2020 did not impact the zooplankton abundance indices on SI since this section is never occupied in spring. Therefore, the record-high value for copepods on SI in 2020 further supports other observations highlighting the high abundance of copepods on the Newfoundland Shelf.

Copepods are mainly herbivores and are key elements of marine food webs, transferring energy from primary producers to higher trophic levels. Large calanoid copepods store energy in the form of lipids before entering diapause — an overwintering dormancy period — making them a high-quality food source preferentially selected by several juvenile and adult fishes (Sameoto et al. 1994; O'Driscoll et al. 2001). Small, less energy-rich copepods are also important prey items for larval and juvenile fish because of their smaller size, high abundance and broad distribution. However, while small calanoid copepods such as *Pseudocalanus* spp. and *Temora longicornis* are often targeted by fish, the cyclopoid *Oithona* spp., is generally selected against, that is, it is consumed in a far lesser proportion than its occurrence in the environment (Pepin and Penney 1997; Heath and Lough 2007). Shifts in zooplankton toward higher abundance of small copepods increases visual constraint and reduce foraging efficiency by predators even under a constant prey biomass scenario (Van Deurs et al. 2015; Ljungström et al. 2020). Consequently, the overall decline in zooplankton biomass and reduction in mean copepod size observed during the 2010s may have negatively impacted the energy transfer to higher trophic levels and contributed to the low productivity of some commercial stocks in the region over the past decade.

The abundance of appendicularians and pteropods shows long-term variation patterns similar to those of small copepods with a transition from below-normal to above-normal levels around 2010 on the Grand Bank, and more variability on the Newfoundland Shelf. The increase in the abundance of bivalve larvae that also occurred in the early 2010s was generalized across the region. Data from the Continuous Plankton Recording (CPR) program also indicated an increase in the relative abundance of dinoflagellates, coccolithophorids, and foraminifera in Grand Bank and Southern Newfoundland waters starting in 2010 (Maillet et al. 2022). Coccolithophores are a primary food source for bivalve larvae (Lindeque et al. 2015) and protists (e.g., flagellates, dinoflagellates, ciliates) may contribute an important fraction of copepod diet (Calbet and Saiz 2005; Castellani et al. 2005). The year 2010–11 was unusually warm in the NL Region with several record-setting seawater temperature indices (Cyr and Galbraith 2021; Cyr et al. 2021). This brief but intense increase in water temperature may have triggered longer-lasting changes in the phytoplankton community with bottom-up effects on mesozooplankton assemblages. However, limited data on long-term variation in phytoplankton community composition in NL waters makes it hard to confirm. Further research is needed to understand the causes of the changes observed in the planktonic environment at the turn of the 2010s.

In addition to the longer-term changes in the size structure of the zooplankton community discussed above, copepod seasonal abundance pattens in 2019 and 2020 also deviated from the climatological means. Near to below normal spring abundances of large *Calanus* spp. at Station 27 in 2019 (no spring data for 2020) resulted in reduced total zooplankton biomass in April and May. On the other hand, late summer and fall abundances of small copepod taxa two to three times higher than average had little impact on biomass. The synchronicity of

biogeochemical cycles and reproduction cycles or predatory organisms is a key mechanism affecting trophic interactions in temperate environments and trophic mismatches can have cascading effects on ecosystem communities (Edwards and Richardson 2004). For example, growth, survival, and recruitment of fish are affected by the timing of seasonal plankton production (Cushing 1990). More research is needed to understand how recent trends of low spring biomass and high abundances of small copepods in the fall observed since the mid-2010s (Maillet et al. 2019, 2022) may have impacted ecosystem productivity in the region.

Timing in the production cycle of *C. finmarchicus* and *Pseudocalanus* spp. copepods at Station 27 in 2019 did not depart strongly from normal conditions. The proportion of adult stages (CVI) was maximum in April (although no data were available for earlier months) while that of newly produced CI-CIV stages peaked between June and August for both species. This aligns with the near-normal timing and duration of the bloom at Station 27 (Head et al. 2000; Broms and Melle 2007). However, the high intensity of the spring bloom at Station 27 may have favoured the faster development of young *C. finmarchicus* stages (i.e., the higher proportion of CIII and CIV stages in July and August) and higher production and/or survival of CI *Pseudocalanus* spp. in May (Pierson et al. 2005). The absence of data from January through July did not permit the characterization the production cycle of young copepodite stages in the spring and early summer of 2020. The distribution pattern of copepodite stages for *Pseudocalanus* spp. was similar to that of the climatology for the July-December period, while the relatively intense fall bloom recorded at Station 27 may have favored the survival of *C. finmarchicus* subadults (CV) and contributed to their high proportion observed from October to December.

Changes in the copepod community composition that occurred in the early 2010s were accompanied by a notable increase in the abundance of some dominant non-copepod taxa such as appendicularians, pteropods and bivalve larvae. These changes in the mesozooplanktonic community suggest that changes also occurred at the smaller planktonic scale (e.g., pico-, nano-, microplankton) that represent the main food source of larger plankton. However, the absence of extensive time series describing the community composition of phytoplankton and other small heterotrophic or mixotrophic organisms for the NL Region limits our ability to identify some of the drivers of these important changes.

4.3. DISSOLVED OXYGEN

DO concentration varies spatially and seasonally, especially in the shallower waters of the continental shelves. The solubility of O_2 in seawater decreases with increasing temperature and salinity and, while photosynthesis by primary producers increase O_2 concentration in surface waters, aerobic processes also use O_2 to decompose the produced organic matter. In some locations, combined effects of warm waters and high recycling rate may result in hypoxia, i.e., O_2 sat level less than 20–30%.

O_2 sat on the NL shelf is generally above 80%. Unlike other part of the Atlantic Zone such as the deeper channels of the Gulf of St. Lawrence, where bottom O_2 sat can reach levels considered harmful for several marine species (Blais et al. 2021a, 2021b), hypoxia has not yet become an issue in NL waters. While low O2 concentrations in the Gulf of St. Lawrence bottom waters are associated with warmer and more saline water masses originating from the entrance Laurentian (Galbraith et al. 2021), the subarctic waters flowing southward along the NL shelf and over the Grand Banks are composed of a mixture of cold, less saline and oxygen-rich water sources originating from the Arctic (Davis Strait, Irminger Sea), the Labrador Sea, and the Hudson Strait. In addition, the annual ventilation resulting from vertical mixing of the water column during the winter months ensure high O_2 sat levels year round, especially for the shallower shelf waters.

Although some indicators (SST, CIL) were indicative of slightly colder-than-normal conditions for the FC section (northern Grand Bank) in 2019, conditions were generally warmer than average on the Newfoundland Shelf in 2019 and throughout the region in 2020 (Cyr and Galbraith 2021; Cyr et al. 2021). Consequently, the strong positive anomalies for O_2 sat observed across most of the water column for SI and FC in 2019 and, to a lesser extent, in 2020 were likely not entirely temperature driven. Changes in the relative contribution of the different water sources forming the subarctic shelf waters that bathe the NL shelves and the Grand Banks could impact O_2 sat levels. More research is needed to fully understand the effect of water circulation on the variability of DO at a Regional level.

4.4. OCEAN ACIDIFICATION

The ocean has absorbed roughly 30% of anthropogenic CO_2 emissions since the industrial revolution making it an important moderator of global warming. As more CO_2 is dissolved in seawater, it reacts to form carbonic acid which acidifies the ocean. OA may, over time, have profound impacts on marine biota and biogeochemical cycles. Ocean pH and calcium carbonate saturation are important indicators of OA. In cold temperate oceans these two metrics are normally in phase but they vary seasonally with temperature and with DIC and alkalinity, which in turn is affected by biological processes such as primary production (Kwiatkowski and Orr 2018).

Seasonal measurements of ocean carbon parameters (TA and DIC) by the AZMP are beginning to identify changes in pH and aragonite saturation levels in Canadian Atlantic waters. Observations reported here and in a previous report by Maillet et al. (2019) indicate that intermediate and near-bottom waters can be undersaturated with aragonite (Ω_a<1) on the Grand Bank during summer and fall, and in deeper slope waters off the Newfoundland Shelf (BB section), the FC, and the southern Grand Bank (SEGB section) in the fall. Earlier studies also identified varying degrees of aragonite undersaturation on the Scotian Shelf (Shadwick and Thomas 2014) and in the St. Lawrence Estuary (Mucci et al. 2011).

The more acidic conditions encountered on the northern Grand Bank generally correspond to shallower areas of the shelf where the CIL strongly interacts with the seafloor (Cyr et al. 2021). Colder waters are normally associated with a lower pH and Ω_a, which may partly explain the higher vulnerability of the northern Grand Bank to OA. The deeper and slightly colder than average CIL on the northern Grand Bank during the summer 2019 (Cyr et al. 2021) may also explain the more acidic conditions observed in summer compared to the fall for that year.

With the forecasted increase in anthropogenic CO_2 emissions, changes in the physical marine environment such as ocean warming and increased stratification together with seasonal variability in phytoplankton production will continue to influence ocean acidity and the saturation state of carbonate minerals into the future. High abundances of acid-sensitive planktonic taxa such as coccolithophorids, foraminifera, pteropods, and bivalve larvae since the early 2010s (Maillet et al. 2022; present report) suggest that OA has not yet become a severe threat for the planktonic community in our Region. However, research showed that non-lethal adverse effects on calcification processes can occur at levels above the saturation threshold of Ω_a=1 (Loucaides et al. 2012; Ries 2012). The long-term effects of these changes to a variety of marine organisms and their impact on plankton community and energy transfer along the food chain is unclear but monitoring of carbonate chemistry and acid-sensitive taxa will remain ongoing within the AZMP.

SUMMARY

- Initiation timing of the spring phytoplankton bloom in 2019 and 2020 was mainly near or earlier than normal across the Region after 4–5 years of mainly later-than-normal blooms.

- There was a general increase in deep nutrient inventories in 2019 and 2020 compared to the previous two years with near- or above-normal levels for nitrate and silicate and near-normal levels for phosphate.
- Chl *a* inventories remained mostly above normal across the NL Region in 2019 for a third consecutive year. The near-normal levels of 2020 can be partly attributed to the missing spring survey and likely represent an underestimation.
- The abundance of both copepod and non-copepod zooplankton remained relatively high in 2019 and 2020 continuing a trend of mostly above-normal abundances that started in the early/mid-2010s.
- Record-high abundances of copepods on the Seal Island and Bonavista Bay sections as well as at Station 27 in 2020 were mainly driven by the high abundances of small *Pseudocalanus* spp. and *Oithona* spp. copepod taxa.
- The abundance of the large calanoid copepod *Calanus finmarchicus* was variable in both years with a record-low value on the Flemish Cap section, and a record-high value on the Seal Island section for the same year.
- Record-highs abundances were observed for bivalve larvae on the SI section in 2019, and for pteropods on SI and at Station 27 in 2020.
- Total zooplankton biomass was mainly near normal across the NL Region for both years except for the second lowest level of the time series on the southeastern Grand Bank section in 2019, and the above-normal levels on the Newfoundland Shelf in 2020.
- DO levels were mainly above 80% throughout most of the NL Region and significantly above-normal across the water column along the Seal Island and Flemish Cap sections in 2019.
- Undersaturated conditions with regards to aragonite (Ω_a<1) were observed on the Grand Bank during summer in 2019, as well as during summer and fall in 2020.

ACKNOWLEDGMENTS

We thank the many scientists and technicians at the Northwest Atlantic Fisheries Centre for the collection and analysis of the samples and the treatment of the data presented in this report as well as the Operational Remote Sensing team at the Bedford Institute of Oceanography who provided access to SST and ocean colour satellite data products. This work would not have been possible without the contribution and expertise of the technicians at the Maurice Lamontagne Institute for the taxonomic identification and counting of zooplankton material. We also thank the captains and crews of the Canadian Coast Guard Ships *Teleost*, *Hudson*, *Alfred Needler*, *Vladykov*, *Amundsen*, and *Earl Grey*, as well as the crew of the British research vessel *RRS James Cook* for oceanographic data collection during 2019 and 2020. We thank Marjolaine Blais, Benoit Casault, and Catherine Johnson for the internal review of the document.

REFERENCES CITED

Blais, M., Galbraith, P.S., Plourde, S., Devred, E., Clay, S., Lehoux, C., and Devine, L. 2021a. Chemical and Biological Oceanographic Conditions in the Estuary and Gulf of St. Lawrence during 2020. DFO Can. Sci. Adv. Sec. Res. Doc. 2021/060. iv + 67 p.

Blais, M., Galbraith, P.S., Plourde, S., Devine, L., and Lehoux, C. 2021b. Chemical and Biological Oceanographic Conditions in the Estuary and Gulf of St. Lawrence during 2019. DFO Can. Sci. Advis. Sec. Res. Doc. 2021/002. iv + 66 p.

Broms, C., and Melle, W. 2007. Seasonal development of *Calanus finmarchicus* in relation to phytoplankton bloom dynamics in the Norwegian Sea. Deep. Res. Part II: Top. Stud. Oceanogr. 54(23–26): 2760–2775.

Buren, A.D., Koen-Alonso, M., Pepin, P., Mowbray, F., Nakashima, B., Stenson, G., Ollerhead, N., and Montevecchi, W.A. 2014. Bottom-Up Regulation of Capelin, a Keystone Forage Species. PLoS One 9(2): 1–11.

Calbet, A., and Saiz, E. 2005. The ciliate-copepod link in marine ecosystems. Aquat. Microb. Ecol. 38(2): 157–167.

Casault, B., Johnson, C., Devred, E., Head, E., Cogswell, A., and Spry, J. 2020. Optical, Chemical, and Biological Oceanographic Conditions on the Scotian Shelf and in the eastern Gulf of Maine during 2019. DFO Can. Sci. Advis. Sec. Res. Doc. 2020/071. v + 64 p.

Casault, B., Johnson, C., Devred, E., Head, E., Beazley, L., and Spry, J. 2022. Optical, Chemical, and Biological Oceanographic Conditions on the Scotian Shelf and in the eastern Gulf of Maine during 2020. DFO Can. Sci. Advis. Sec. Res. Doc. 2022/018. v + 82 p.

Castellani, C., Irigoien, X., Harris, R.P., and Lampitt, R.S. 2005. Feeding and egg production of *Oithona similis* in the North Atlantic. Mar. Ecol. Prog. Ser. 288: 173–182.

Chen, B., Cai, W.-J., and Chen, L. 2015. The marine carbonate system of the Arctic Ocean: Assessment of internal consistency and sampling considerations, summer 2010. Mar. Chem. 176: 174–188.

Clay, S., Layton, C., and Devred, E. 2021. BIO-RSG/PhytoFit: First release. v1.0.0. Zenodo.

Clay, S., Peña, A., DeTracey, B., and Devred, E. 2019. Evaluation of Satellite-Based Algorithms to Retrieve Chlorophyll-a Concentration in the Canadian Atlantic and Pacific Oceans. Remote Sens. 11(22): 1–29.

Craig, S.E., Thomas, H., Jones, C.T., Li, W.K.W., Greenan, B.J.W., Shadwick, E.H., and Burt, W.J. 2015. The effect of seasonality in phytoplankton community composition on CO_2 uptake on the Scotian Shelf. J. Mar. Syst. 147: 52–60.

Cushing, D.H. 1990. Plankton Production and Year-class Strength in Fish Populations: an Update of the Match/Mismatch Hypothesis. Advances Mar. Biol. 26: 249–293.

Cyr, F., Bourgault, D., and Galbraith, P.S. 2011. Interior versus boundary mixing of a cold intermediate layer. J. Geophys. Res. Oceans. 116(C12): 12 p.

Cyr, F., and Galbraith, P.S. 2021. A climate index for the Newfoundland and Labrador shelf. Earth Syst. Sci. Data. 13(5): 1807–1828.

Cyr, F., Snook, S., Bishop, C., Galbraith, P.S., Pye, B., Chen, N., and Han, G. 2021. Physical Oceanographic Conditions on the Newfoundland and Labrador Shelf during 2019. DFO Can. Sci. Advis. Sec. Res. Doc. 2021/017. iv + 52 p.

Dauchez, S., Legendre, L., Fortier, L., and Levasseur, M. 1996. Nitrate uptake by size-fractionated phytoplankton on the Scotian Shelf (Northwest Atlantic): spatial and temporal variability. J. Plankton Res. 18(4): 577–595.

DFO. 2020. Oceanographic Conditions in the Atlantic Zone in 2019. DFO Can. Sci. Advis. Sec. Sci. Advis. Rep. 2020/028.

DFO. 2021. Oceanographic Conditions in the Atlantic Zone in 2020. DFO Can. Sci. Advis. Sec. Sci. Advis. Rep. 2021/026.

Dickson, A.G. 1990. Standard potential of the reaction: AgCl(s) + 1.2H_2(g) = Ag(s) + HCl (aq), and the standard acidity constant of the ion HSO_4^- in synthetic sea water from 273.15 to 318.15 K. J. Chem. Thermodynamics. 22(2): 113–127.

Dickson, A.G., and Millero, F.J. 1987. A comparison of the equilibrium constants for the dissociation of carbonic acid in seawater media. Deep Sea Res. Part A. Oceanogr. Res. Papers. 34(10): 1733–1743.

Dickson, A.G., Sabine, C.L., and Christian, J.R. (Eds.). 2007. Guide to best practices for ocean CO_2 measurements. PICES Spec. Pub. 3: 191 pp.

Durant, J.M., Anker-Nilssen, T., and Stenseth, N.C. 2003. Trophic interactions under climate fluctuations: the Atlantic puffin as an example. Proc. R. Soc. Lond. B. 270(1523): 1461–1466.

Edwards, M., and Richardson, A.J. 2004. Impact of climate change on marine pelagic phenology an trophic mismatch. Nature. 430: 881–884.

Florindo-López, C., Bacon, S., Aksenov, Y., Chafik, L., Colbourne, E., and Penny Holliday, N.P. 2020. Arctic Ocean and Hudson Bay Freshwater Exports: New Estimates from Seven Decades of Hydrographic Surveys on the Labrador Shelf. J. Clim. 33(20): 8849–8868.

Galbraith, P.S., Chassé, J., Shaw, J.-L., Dumas, J., Caverhill, C., Lefaivre, D., and Lafleur, C. 2021. Physical Oceanographic Conditions in the Gulf of St. Lawrence during 2020. DFO Can. Sci. Advis. Sec. Res. Doc. 2021/045. iv + 81 p.

Head, E.J.H., Harris, L.R., and Campbell, R.W. 2000. Investigations on the ecology of *Calanus* spp. in the Labrador Sea. I. Relationship between the phytoplankton bloom and reproduction and development of *Calanus finmarchicus* in spring. Mar. Ecol. Prog. Ser. 193: 53–73.

Head, E.J.H., Harris, L.R., and Yashayaev, I. 2003. Distributions of *Calanus* spp. and other mesozooplankton in the Labrador Sea in relation to hydrography in spring and summer (1995–2000). Prog. Oceanogr. 59(1): 1–30.

Heath, M.R., and Lough, R.G. 2007. A synthesis of large-scale patterns in the planktonic prey of larval and juvenile cod (*Gadus morhua*). Fish. Oceanogr. 16(2): 169–185.

Hlista, B.L., Sosik, H.M., Traykovski, L.V.M., Kenney, R.D., and Moore, M.J. 2009. Seasonal and interannual correlations between right-whale distribution and calving success and chlorophyll concentrations in the Gulf of Maine, USA. Mar. Ecol. Prog. Ser. 394: 289–302.

Horwood, J.W., Nichols, J.H., and Harrop, R. 1982. Seasonal Changes in Net Phytoplankton of the West-Central North Sea. J. Mar. Biol. Assoc. UK. 62(1): 15–23.

Howarth, R.W. 1988. Nutrient Limitation of Net Primary Production in Marine Ecosystems. 19: 89–110.

Humphreys, M.P., Lewis, E.R., Sharp, J.D., and Pierrot, D. 2022. PyCO2SYS v1.8: marine carbonate system calculations in Python. Geosci. Model Devel. 15(1): 15–43.

Joyce, T.M., Hernandez-Guerra, A., and Smethie, W.M. 2001. Zonal circulation in the NW Atlantic and Caribbean from a meridional World Ocean Circulation Experiment hydrographic section at 66°W. J. Geophys. Res. Oceans. 106(C10): 22095–22113.

Koen-Alonso, M., Pepin, P., Fogarty, M.J., Kenny, A., and Kenchington, E. 2019. The Northwest Atlantic Fisheries Organization Roadmap for the development and implementation of an Ecosystem Approach to Fisheries: structure, state of development, and challenges. Mar. Policy. 100: 342–352.

Krause, J.W., Schulz, I.K., Rowe, K.A., Dobbins, W., Winding, M.H.S., Sejr, M.K., Duarte, C.M., and Agustí, S. 2019. Silicic acid limitation drives bloom termination and potential carbon sequestration in an Arctic bloom. Sci. Rep. 9(8149): 1–11.

Krauss, W., KäSe, R.H., and Hinrichsen, H.-H. 1990. The branching of the Gulf Stream southeast of the Grand Banks. J. Geophys. Res. Oceans. 95(C8): 13089–13103.

Kristiansen, T., Drinkwater, K.F., Lough, R.G., and Sundby, S. 2011. Recruitment Variability in North Atlantic Cod And Match-Mismatch Dynamics. PLoS One 6(3): e17456.

Kwiatkowski, L., and Orr, J.C. 2018. Diverging seasonal extremes for ocean acidification during the twenty-first century. Nat. Clim. Change. 8(2): 141–145.

Lewis, E., Wallace, D., and Allison, L.J. 1998. Program developed for CO{sub 2} system calculations. United States.

Lindeque, P.K., Dimond, A., Harmer, R.A., Parry, H.E., Pemberton, K.L., and Fileman, E.S. 2015. Feeding selectivity of bivalve larvae on natural plankton assemblages in the Western English Channel. Mar. Biol. 162(2): 291–308.

Ljungström, G., Claireaux, M., Fiksen, Ø., and Jørgensen, C. 2020. Body size adaptions under climate change: zooplankton community more important than temperature or food abundance in model of a zooplanktivorous fish. Mar. Ecol. Prog. Ser. 636: 1–18.

Loucaides, S., Poulton, A.J., Bellerby, R., and Tyrrell, T. 2012. Coccolithophore community composition and calcification rates in the Norwegian and Greenland seas as a function of carbonate chemistry and other environmental parameters. EGU General Assembly 2012, held 22-27 April 2012 in Vienna, Austria. 11407.

Maillet, G., Bélanger, D., Doyle, G., Robar, A., Fraser, S., Higdon, J., Ramsay, D., and P. Pepin. 2019. Optical, Chemical, and Biological oceanographic conditions on the Newfoundland and Labrador Shelf during 2016-2017. DFO Can. Sci. Advis. Sec. Res. Doc. 2019/055.viii + 35 p.

Maillet, G., Bélanger, D., Doyle, G., Robar, A., Rastin, S., Ramsay, D., and Pepin, P. 2022. Optical, Chemical, and Biological Oceanographic Conditions on the Newfoundland and Labrador Shelf during 2018. DFO Can. Sci. Advis. Sec. Res. Doc. 2022/075. viii + 53 p.

McDougall, T.J., and Barker, P.M. 2011. Getting started with TEOS-10 and the Gibbs Seawater (GSW) Oceanographic Toolbox. SCOR/IAPSO WG.127. 1–28.

Mehrbach, C., Culberson, C.H., Hawley, J.E., and Pytkowicx, R.M. 1973. Measurement of the Apparent Dissociation Constants of Carbonic Acid in Seawater At Atmospheric Pressure. Limnol. Oceanogr. 18(6): 897–907.

Mitchell, M.R., G. Harrison, K. Pauley, A. Gagné, G. Maillet, and P. Strain. 2002. Atlantic Zonal Monitoring Program Sampling Protocol. Can. Tech. Rep. Hydrogr. Ocean Sci. 223: iv + 23 pp.

Mucci, A., Starr, M., Gilbert, D., and Sundby, B. 2011. Acidification of Lower St. Lawrence Estuary Bottom Waters. Atmos. – Ocean. 49(3): 206–218.

Mullowney, D., Maillet, G., Dawe, E., Rose, G., and Rowe, S. 2016. Spawning delays of northern capelin (Mallotus villosus) and recovery dynamics: A mismatch with ice-mediated spring bloom? Prog. Oceanogr. 141: 144–152.

O'Driscoll, R.L., Parsons, M.J.D., and Rose, G.A. 2001. Feeding of capelin (*Mallotus villosus*) in Newfoundland waters. Sarsia. 86(3): 165–176.

Orr, J.C., J.-M., E., and Gattuso, J.-P. 2015. Comparison of ten packages that compute ocean carbonate chemistry. Biogeosciences. 12: 1483–1510.

Pepin, P., Colbourne, E., and Maillet, G. 2011. Seasonal patterns in zooplankton community structure on the Newfoundland and Labrador Shelf. Prog. Oceanogr. 91(3): 273–285.

Pepin, P. and Penney, R.W. 1997. Patterns of prey size and taxonomic composition in larval fish: Are there general size-dependent models? J. Fish Biol. 51: 84–100.

Petrie, B., Akenhead, B., Lazier, J., and Loder, J. 1988. The cold intermediate layer on the Labrador and Northeast Newfoundland shelves, 1978-1986. NAFO Sci. Coun. Stud. 12: 57–69.

Pierson, J.J., Leising, A.W., Halsband-Lenk, C., and Ferm, N. 2005. Vertical distribution and abundance of *Calanus pacificus* and *Pseudocalanus newmani* in relation to chlorophyll *a* concentrations in Dabob Bay, Washington. Prog. Oceanogr. 67: 349–365.

Planque, B., and Batten, S.D. 2000. *Calanus finmarchicus* in the North Atlantic: The year of *Calanus* in the context of interdecadal change. ICES J. Mar. Sci. 57(6): 1528–1535.

Regular, P.M., Hedd, A., Montevecchi, W.A., Robertson, G.J., Storey, A.E., and Walsh, C.J. 2014. Why timing is everything: Energetic costs and reproductive consequences of resource mismatch for a chick-rearing seabird. Ecosphere. 5(12): 1–13.

Ries, J.B. 2012. A sea butterfly flaps its wings. Nat. Geosci. 5(12): 845–846.

Sameoto, D., Neilson, J., and Waldron, D. 1994. Zooplankton prey selection by juvenile fish in Nova Scotian Shelf basins. J. Plankton Res. 16(8): 1003–1019.

Shadwick, E.H., and Thomas, H. 2014. Seasonal and spatial variability in the CO2 system on the Scotian Shelf (Northwest Atlantic). Mar. Chem. 160: 42–55.

Therriault, J.-C., B. Petrie, P. Pepin, J. Gagnon, D. Gregory, J. Helbig, A. Herrnan, D. Lefaivre, M. Mitchell, B. Pelchat, J. Runge, and D. Sarneoto. 1998. Proposal for a northwest Atlantic zonal monitoring program. Can. Tech. Rep. Hydrogr. Ocean Sci. 194: vii+57 p.

Townsend, D.W., Cammen, L.M., Holligan, P.M., Campbell, D.E., and Pettigrew, N.R. 1994. Causes and consequences of variability in the timing of spring phytoplankton blooms. Deep. Res. Part I 41(5–6): 747–765.

Townsend, D.W., Thomas, A.C., Mayer, L.M., Thomas, M., and Quinlan, J. 2004. Oceanography of the northwest Atlantic continental shelf. Sea Glob. Coast. Ocean Interdiscip. Reg. Stud. Synth. (June): 119–168.

Uppstrom, L.R. 1974. The boron/chlorinity ratio of deep-sea water from the Pacific Ocean. Deep. Res. 21: 161–162.

Van Deurs, M., Jorgensen, C., and Fiksen, O. 2015. Effects of copepod size on fish growth: a model based on data for North Sea sandeel. Mar. Ecol. Prog. Ser. 520: 235–243.

Wang, Z., Yashayaev, I., and Greenan, B. 2015. Seasonality of the inshore Labrador current over the Newfoundland shelf. Cont. Shelf Res. 100: 1–10.

Winkler, L. 1888. Die Bestimmung des im Wasser gelosten Sauerstoffes. Berichte der Dtsch. Chem. Gesellschaft 21(2): 2843–2854.

Wu, Y., Peterson, I.K., Tang, C.C.L., Platt, T., Sathyendranath, S., and Fuentes-Yaco, C. 2007. The impact of sea ice on the initiation of the spring bloom on the Newfoundland and Labrador Shelves. J. Plankton Res. 29(6): 509–514.

Zhai, L., Platt, T., Tang, C., Sathyendranath, S., and Hernández Walls, R. 2011. Phytoplankton phenology on the Scotian Shelf. ICES J. Mar. Sci. 68(4): 781–791.

APPENDIX I - TABLES

Table 1: Summary of biogeochemical sampling effort in the Newfoundland and Labrador Region in 2019 and 2020 during Atlantic Zone Monitoring Program (AZMP) seasonal surveys along the Seal Island (SI), Bonavista Bay (BB), Flemish Cap (FC), and southeastern Grand Bank (SEGB) oceanographic sections as well as at the high-frequency monitoring site Station 27 (S27) by ships of opportunity (SOO).

				Collected samples				
Year	Survey	Section	Occupied stations	Nutrients	Chl *a*	Zooplankton	Dissolved O_2	Carbonates
2019	Spring	FC	31	225	187	24	58	93
	Summer	SI	14	109	86	11	32	87
	-	BB	15	136	102	13	39	84
	-	FC	33	225	187	23	59	135
	Fall	BB	14	139	111	14	44	73
	-	FC	24	227	185	24	49	95
	-	SEGB	15	130	111	15	36	50
	SOO	S27	44	202	212	32	-	57
	Total	**-**	**190**	**1,393**	**1,181**	**156**	**317**	**674**
2020	Summer	SI	14	110	84	11	32	55
	-	BB	14	138	100	13	40	71
	-	FC	33	229	186	23	59	91
	Fall	BB	15	149	107	14	40	80
	-	FC	35	230	187	24	59	93
	-	SEGB	21	122	106	15	36	47
	SOO	S27	27	181	173	21	-	48
	Total	**-**	**159**	**1,159**	**943**	**121**	**266**	**485**

APPENDIX II - FIGURES

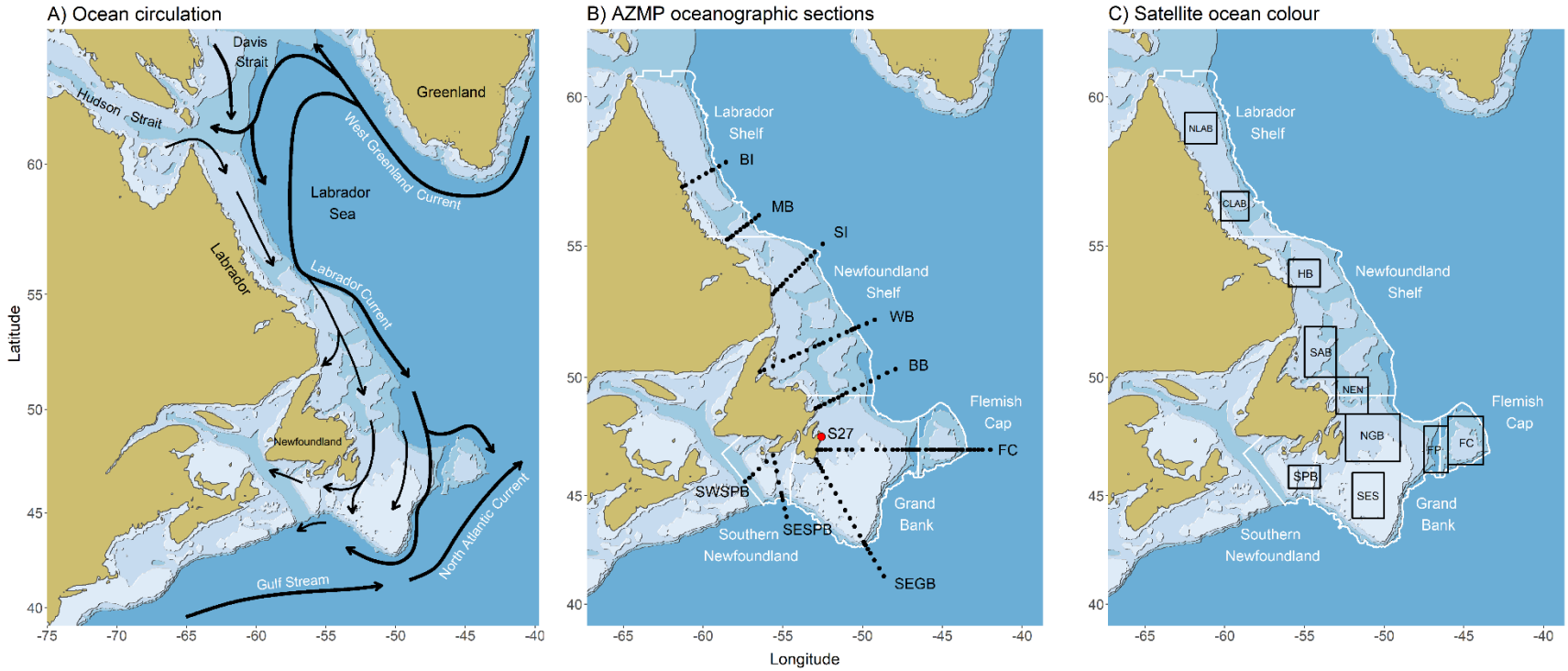

Figure 1: A) Water circulation in the Newfoundland and Labrador Region. B) Location of AZMP standard cross-shelf oceanographic sections (BI=Beachy Island, MB=Makkovik Bank, SI=Seal Island, WB=White Bay, BB=Bonavista Bay, FC=Flemish Cap, SEGB=Southeastern Grand Bank, SWSPB=Southwest St. Pierre Bank, SESPB=Southeast St. Pierre Bank) and high-frequency monitoring site Station 27 (S27) occupied by the AZMP since 1999 in the Newfoundland and Labrador Region. Black dots represent sampling stations along each section. C) Location of the subregions for which spring phytoplankton bloom indices (timing, duration and magnitude) were calculated using satellite ocean colour data (NLAB=Northern Labrador, CLAB=Central Labrador, HB=Hamilton Bank, SAB=St. Anthony Basin, NEN=Northeast Newfoundland, NGB=Northern Grand Bank, FP=Flemish Pass, FC=Flemish Cap, SES=Southeast Shoal, SPB=St. Pierre Bank). NAFO's Ecosystem Production Units (EPUs) used in this report to refer to the different subregions of the Newfoundland and Labrador continental shelf are indicated in white in panels B and C.

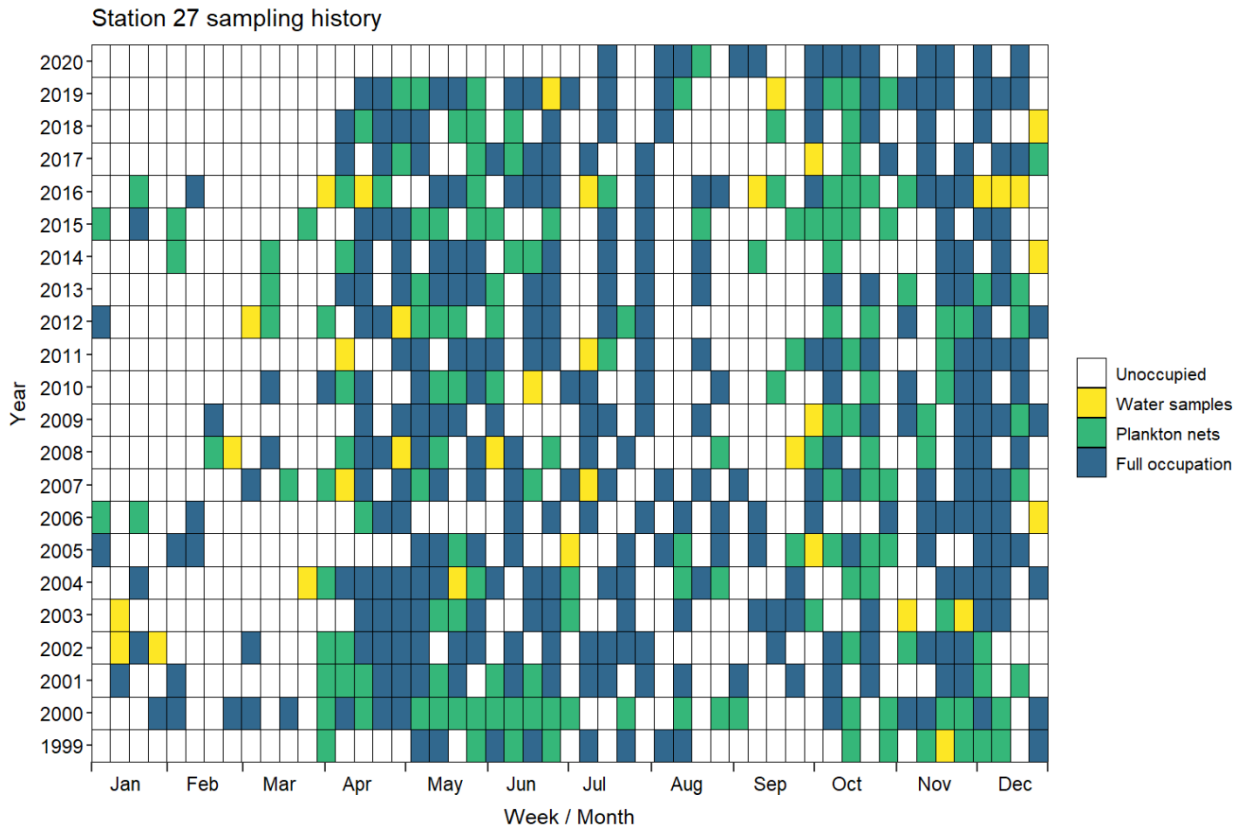

Figure 2: Summary of weekly biogeochemical sampling activities at the high-frequency monitoring site Station 27 (S27) since the start of AZMP in 1999. Coloured cells indicate weeks when at least one occupation occurred and during which water (yellow cells), plankton (green cells) or water and plankton (blue cells) were collected. CTD casts were performed on each occupation.

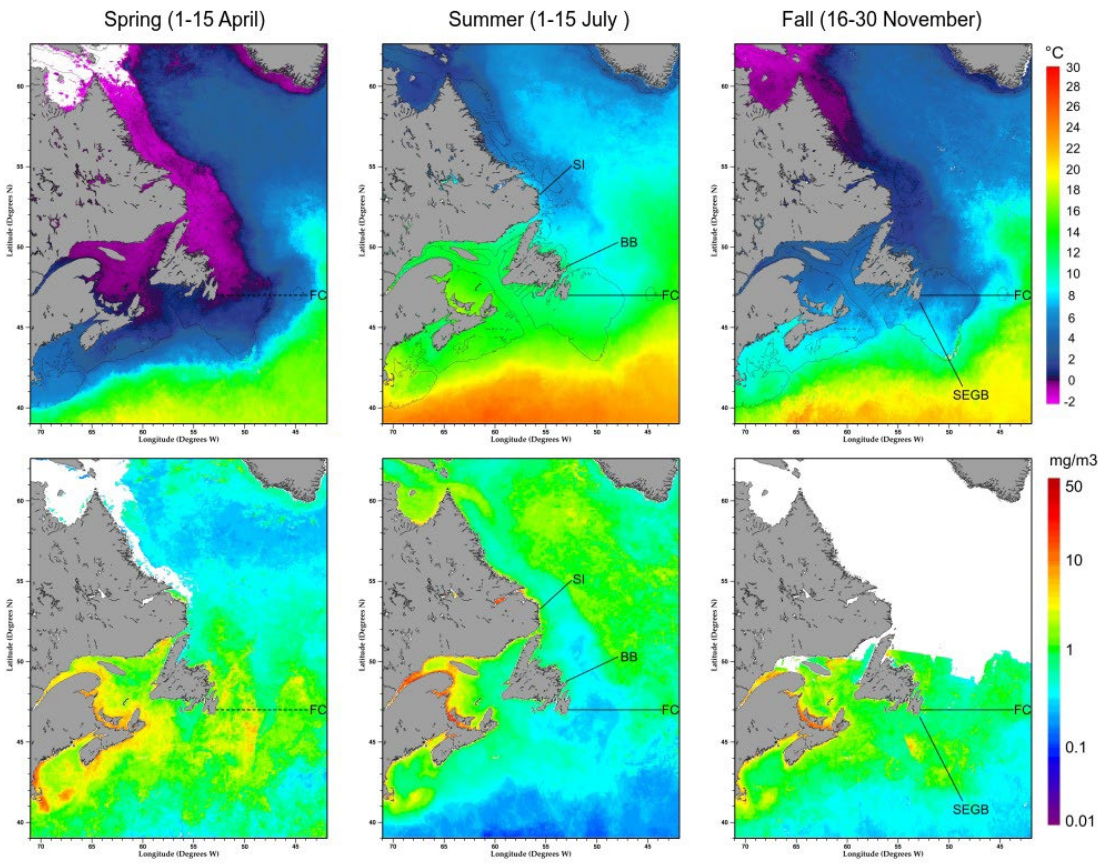

Figure 3: Long-term average (2003-20) sea surface temperature (top) and surface chlorophyll a concentration (bottom) conditions prevailing in the Newfoundland Region during the spring (left), summer (middle), and fall (right) AZMP surveys. Dashed lines indicate oceanographic sections occupied in 2019 only. Solid lines indicates sections occupied in both 2019 and 2020. White indicate location where data was not available because of sea ice, cloud cover or, in the case of chlorophyll in the fall, limited daylight hours at appropriate incidence angle.

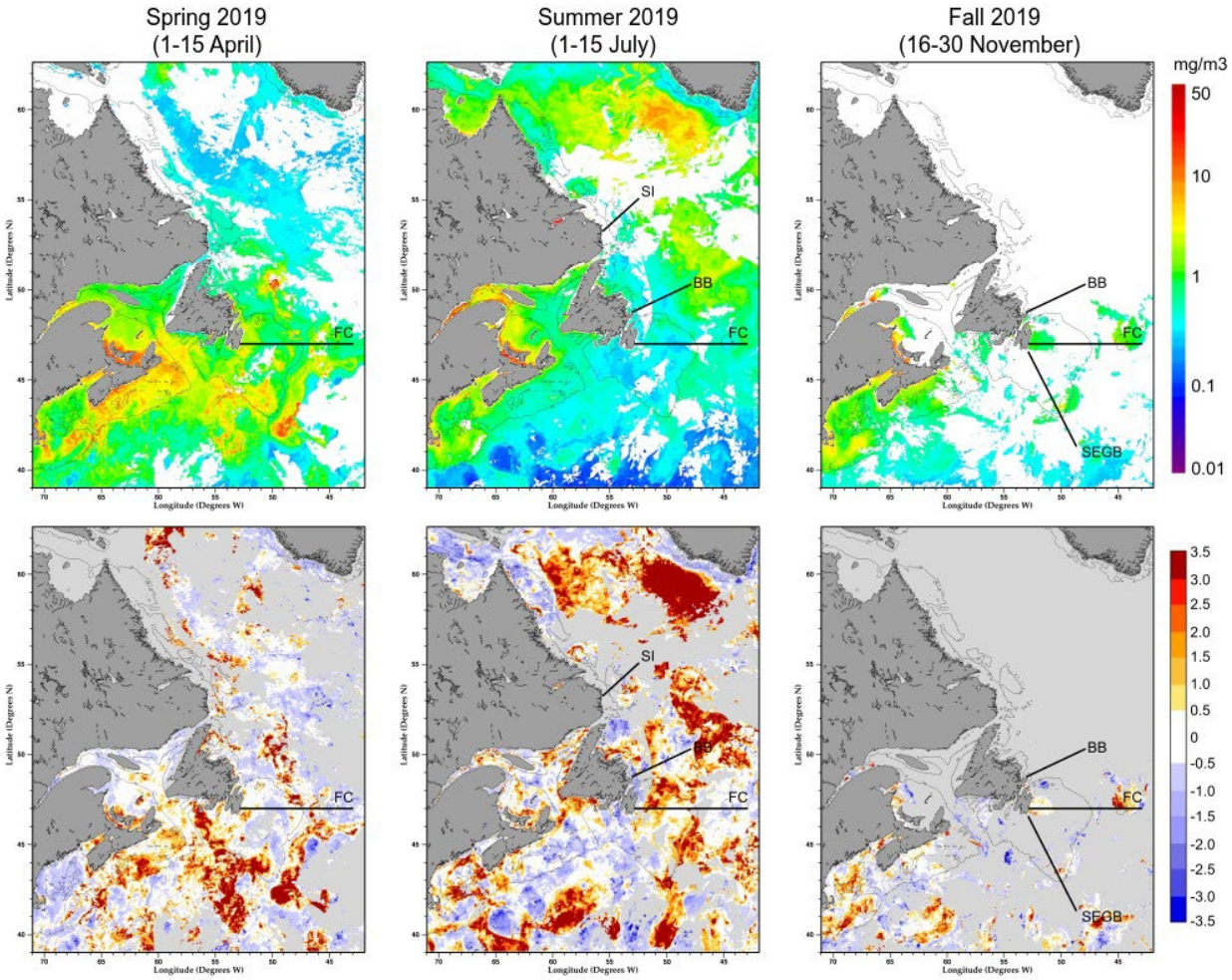

Figure 4: Mean surface chlorophyll a concentration (top) and standardized anomalies (bottom) during the 2019 AZMP seasonal surveys. The black lines indicate oceanographic sections occupied in 2019. In the bottom panels, white indicates near-normal levels (i.e., ± 0.5 SD from climatological mean), blue (red) shades indicate below-normal (above-normal) levels, and grey indicates locations where data was not available because of sea ice, cloud cover or limited daylight hours at appropriate incidence angle. Anomalies were calculated using a 2003–20 climatology.

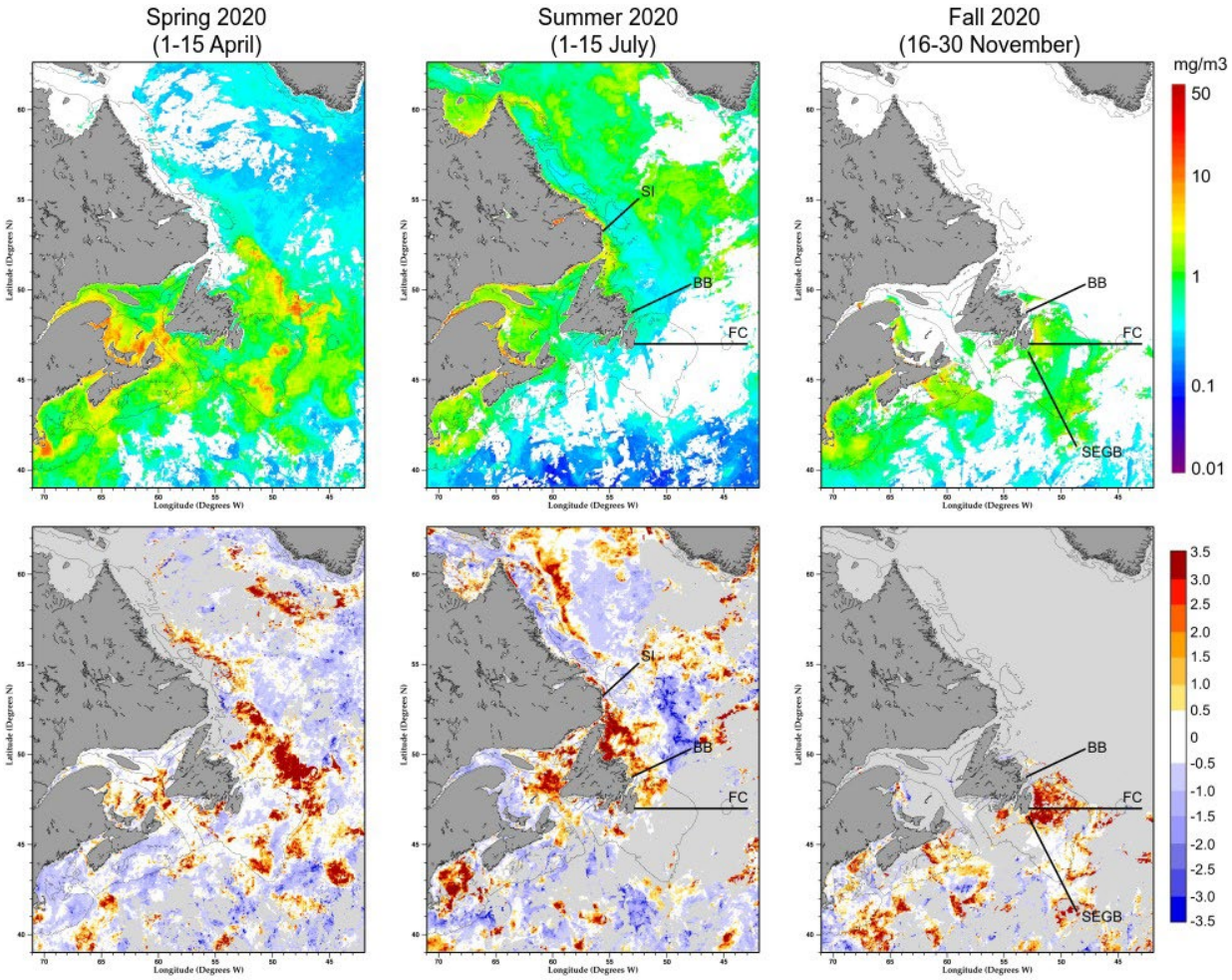

Figure 5: Mean surface chlorophyll-a concentration (top) and standardized anomalies (bottom) during the 2020 AZMP seasonal surveys. In the bottom panels, white indicates near normal levels (i.e., ± 0.5 SD from climatological mean), blue (red) shades indicate below-normal (above-normal) levels. Light grey indicates locations where data was not available because of sea ice, cloud cover or limited daylight hours at appropriate incidence angle. Anomalies were calculated using a 2003–20 climatology.

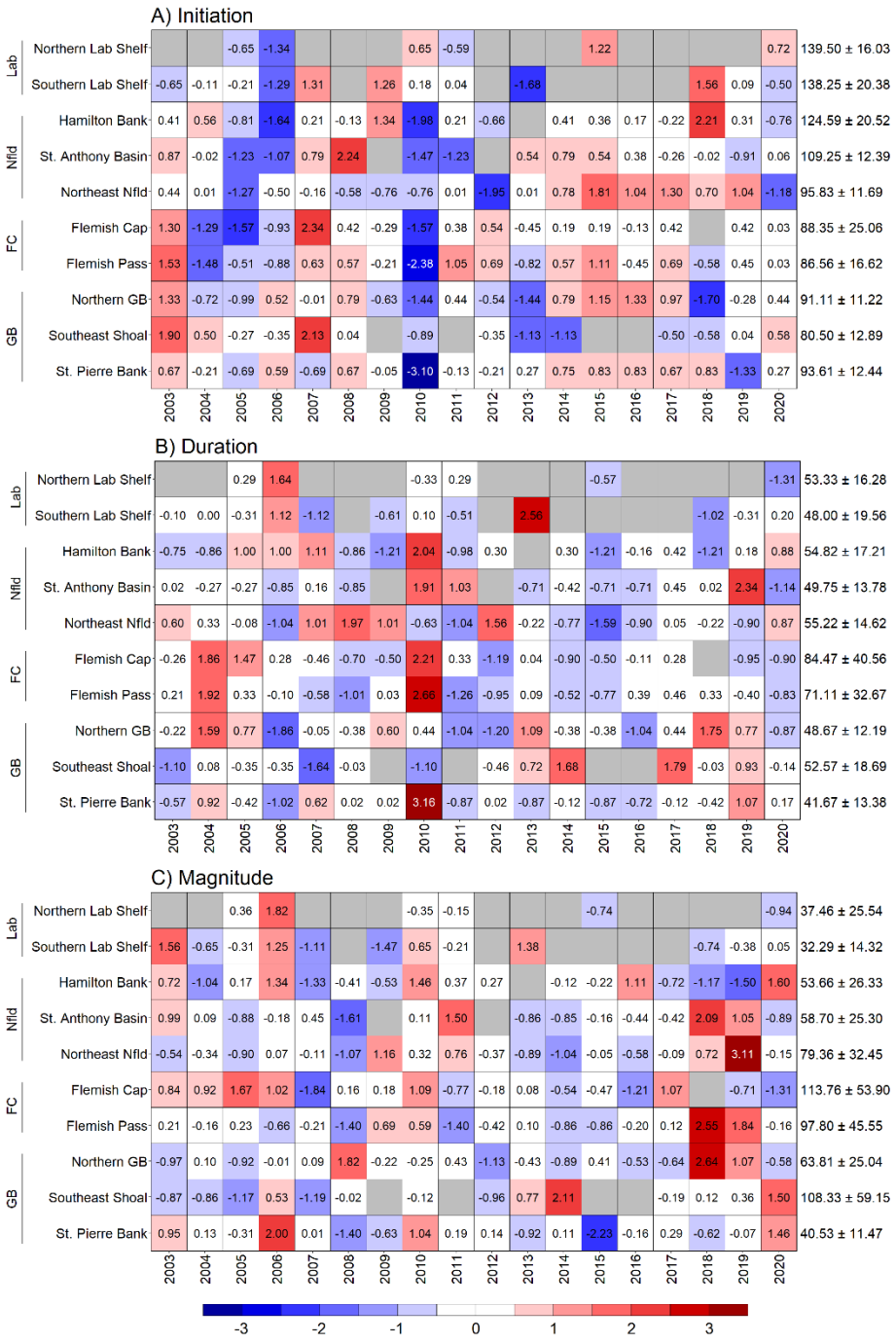

Figure 6: Annual anomaly scorecards for the spring phytoplankton bloom metrics. Numbers in each cell are standardized anomalies in standard deviation (SD) units. White cells indicate near-normal conditions, i.e., ± 0.5 SD relative to the climatological mean. Blue (red) cells indicate earlier (later) initiation, shorter (longer) duration, or lower (higher) magnitude than normal. Grey cells indicate missing data. Climatological means and SD for the 2003–20 reference period are listed to the right in units of day of year (initiation), number of days (duration) and in mg·m-2·d-1 (magnitude).

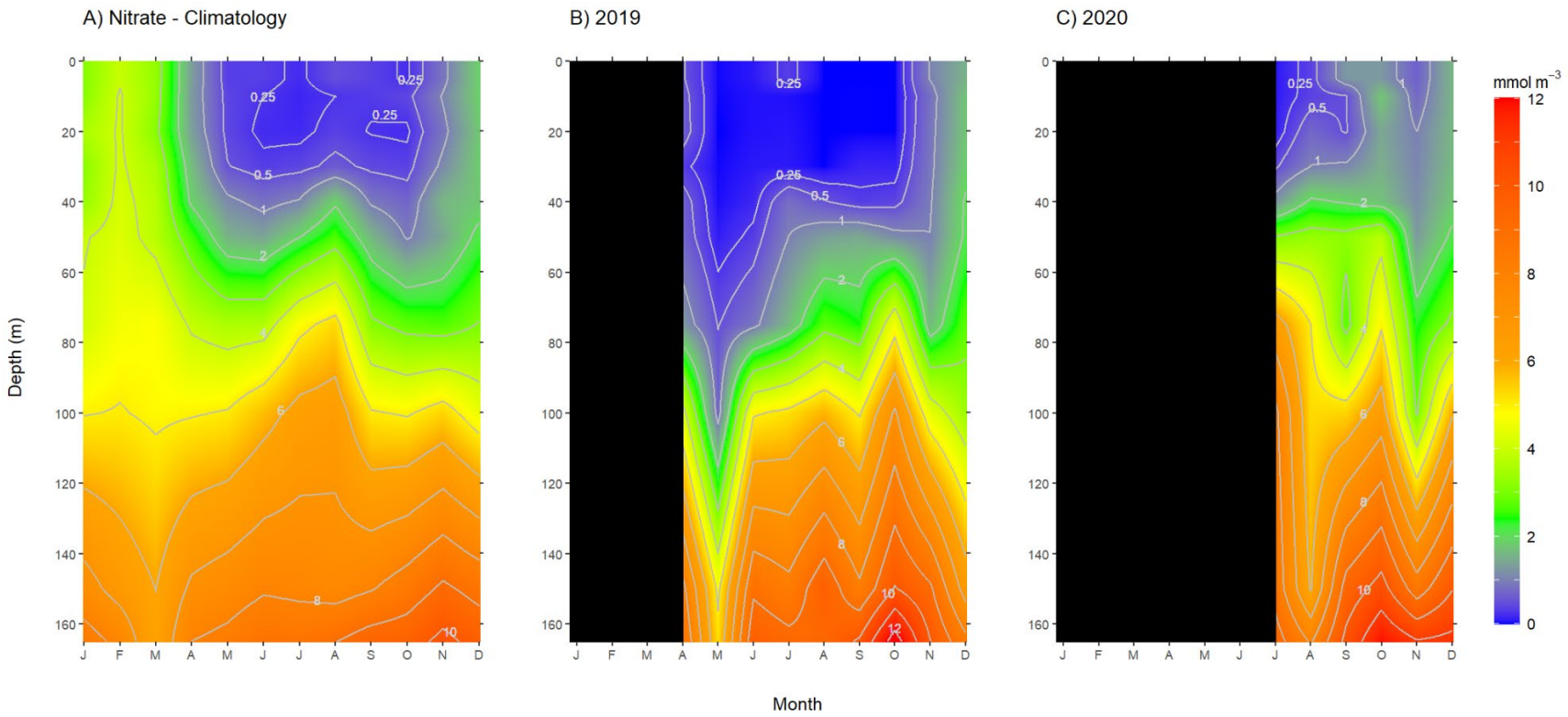

Figure 7: Seasonal variations in the vertical distribution of nitrate at Station 27. Monthly mean concentrations were calculated for each water collection depth (5, 10, 20, 30, 40, 50, 75, 100, 150 m, bottom) and interpolated across depth and time. Climatological means were calculated using a 1999–2020 reference period. Black rectangles indicate time of year when data was not available.

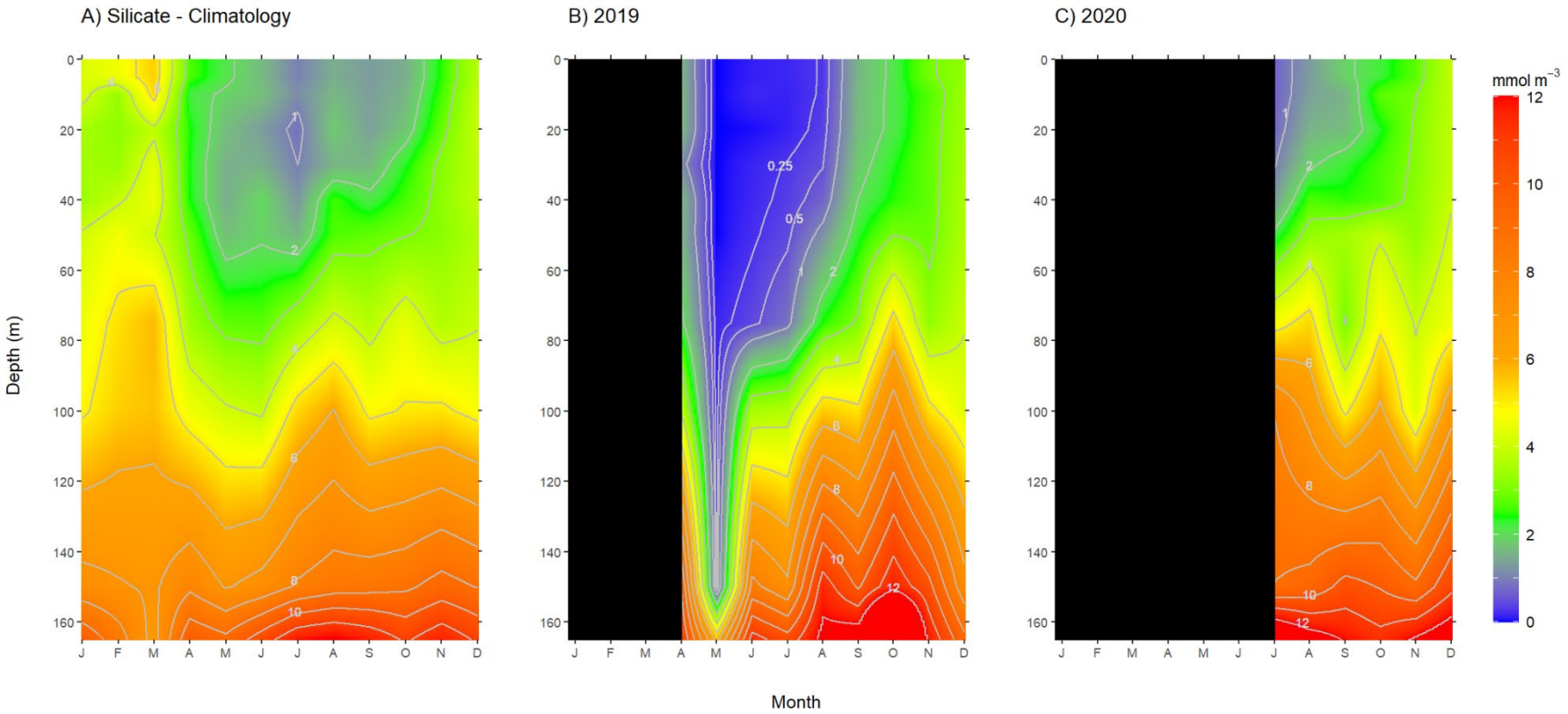

Figure 8: Seasonal variations in the vertical distribution of silicate at Station 27. Monthly mean concentrations were calculated for each water collection depths (5, 10, 20, 30, 40, 50, 75, 100, 150 m, bottom) and interpolated linearly across depth and time. Climatological means were calculated using a 1999–2020 period. Black rectangles indicate time of year when data was not available.

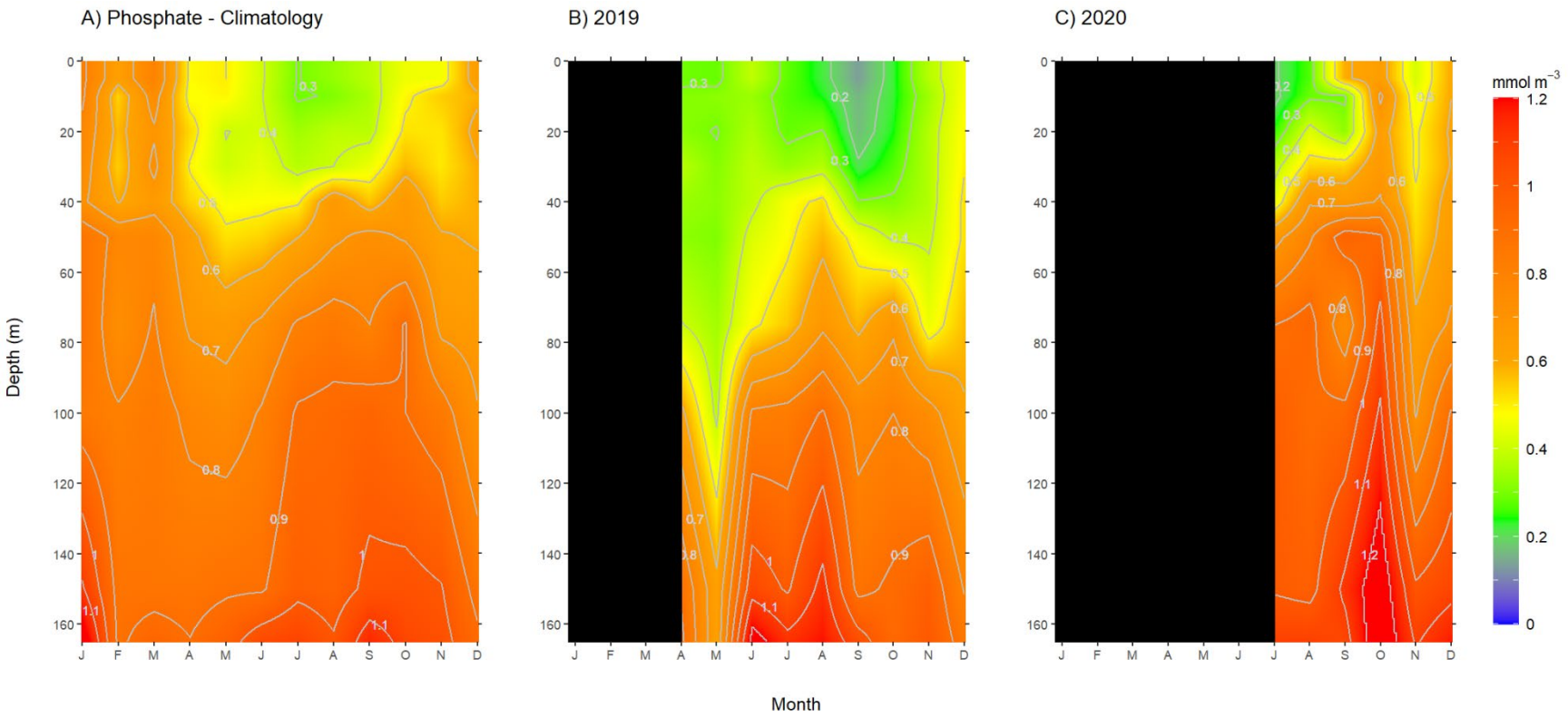

Figure 9: Seasonal variations in the vertical distribution of phosphate at Station 27. Monthly mean concentrations were calculated for each water collection depths (5, 10, 20, 30, 40, 50, 75, 100, 150 m, bottom) and interpolated linearly across depth and time. Climatological means were calculated using a 1999–2020 period. Black rectangles indicate time of year when data was not available.

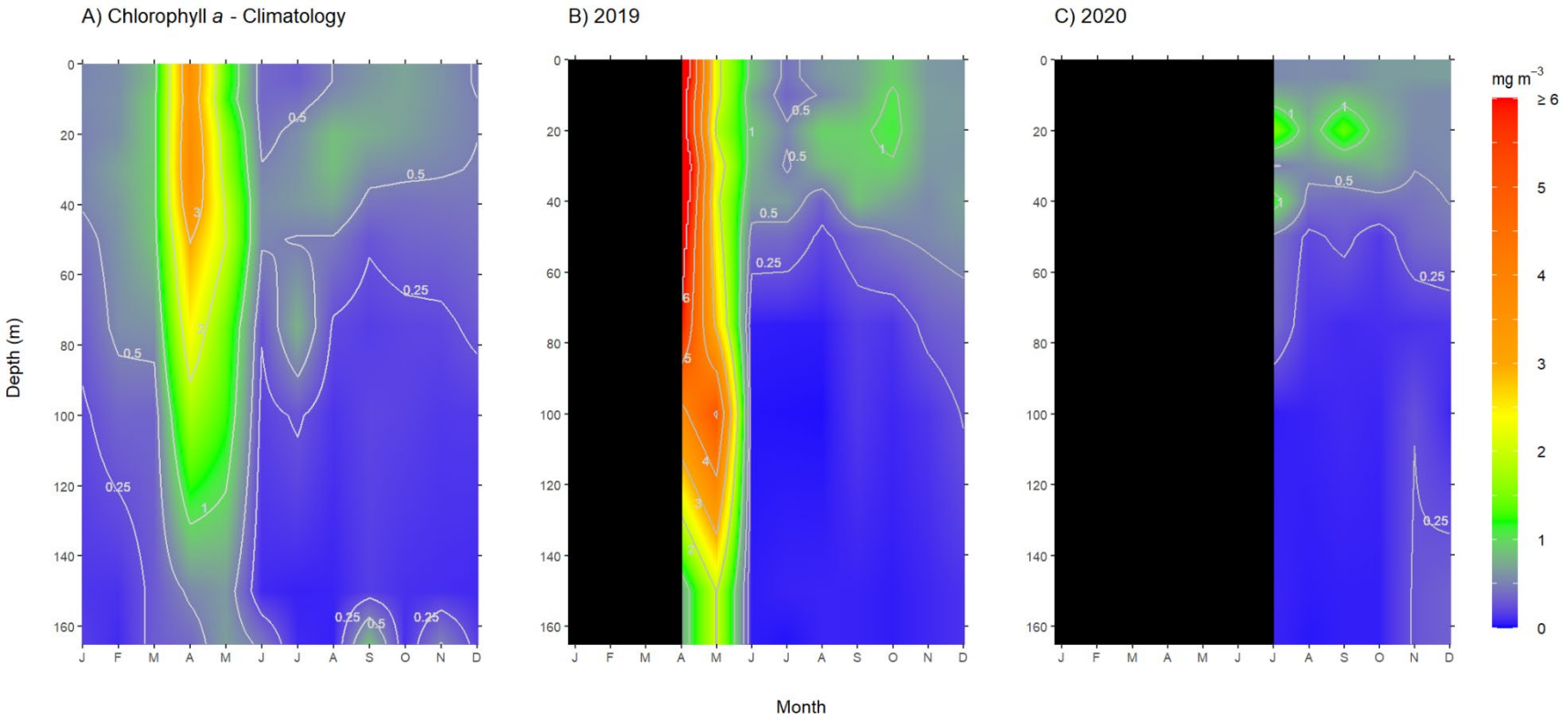

Figure 10: Seasonal variation in the vertical distribution of chlorophyll at Station 27. Monthly mean concentrations were calculated for each water collection depths (5, 10, 20, 30, 40, 50, 75, 100, 150 m, bottom) and interpolated linearly across depth and time. Climatological means were calculated using a 1999–2020 period. Black rectangles indicate time of year when data was not available.

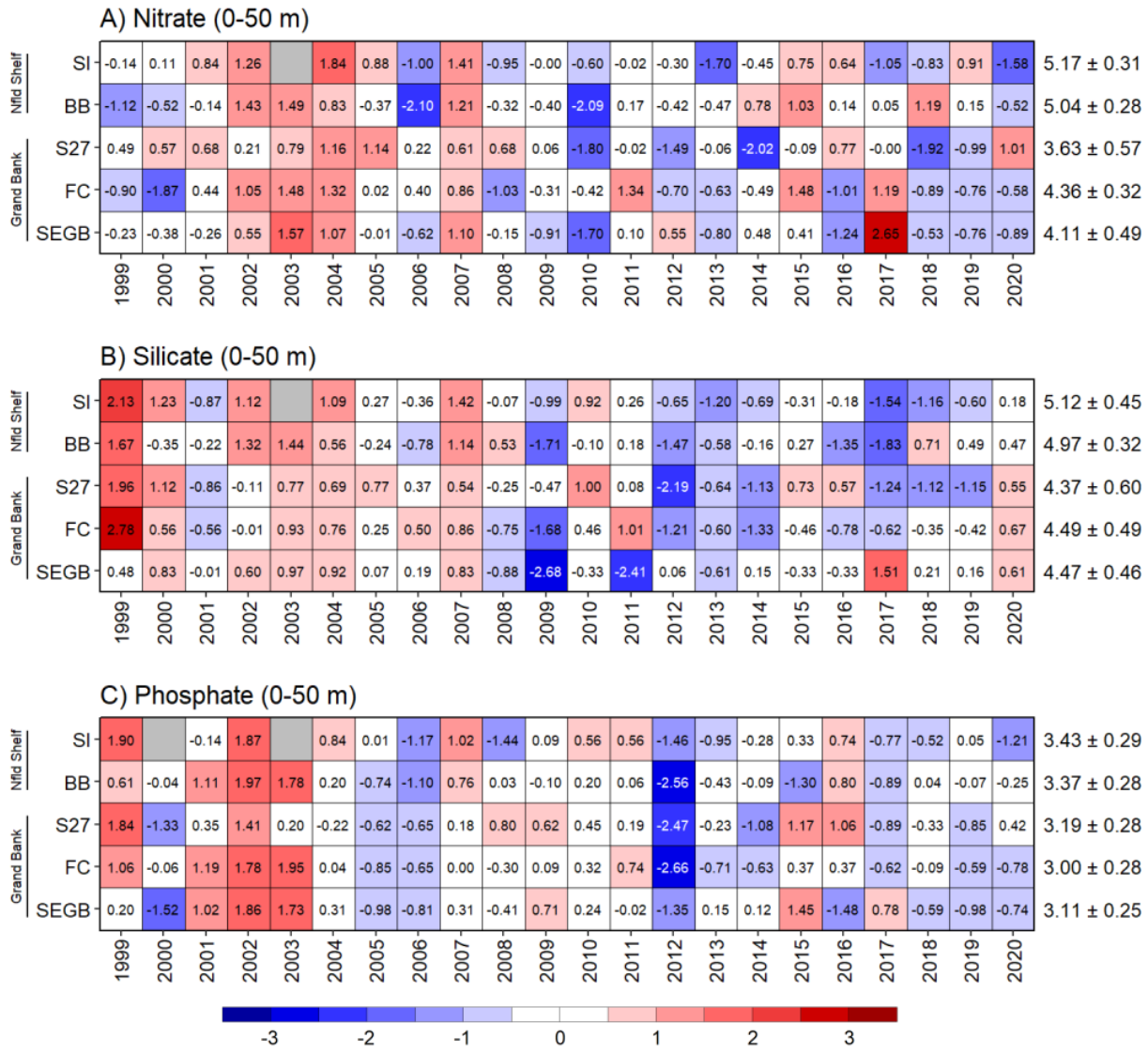

Figure 11: Annual anomaly scorecards for the shallow nutrient inventories. Numbers in cells are standardized anomalies in standard deviation (SD) units. White cells indicate near-normal conditions, i.e., ± 0.5 SD relative to the climatological mean. Blue (red) cells indicate lower (higher) concentration than normal. Grey cells indicate missing data. Climatological means and SD for the 1999–2020 reference period are listed to the right in units of ln(1+concentration in mmol·m-2).

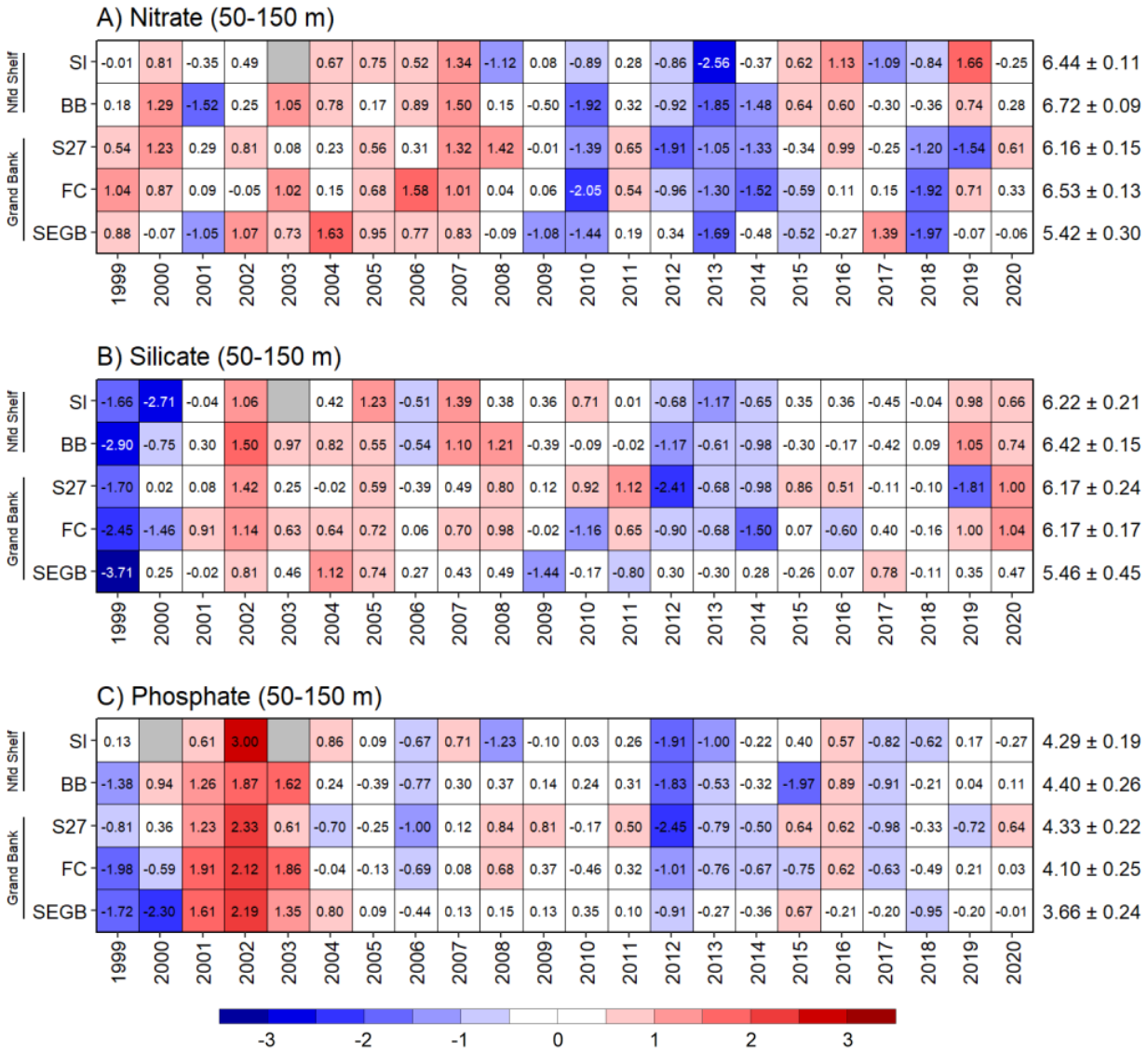

Figure 12: Annual anomaly scorecards for the deep nutrient inventories. Numbers in cells are standardized anomalies in standard deviation (SD) units. White cells indicate near-normal conditions, i.e., ± 0.5 SD relative to the climatological mean. Blue (red) cells indicate lower (higher) concentration than normal. Grey cells indicate missing data. Climatological means and SD for the 1999–2020 reference period are listed to the right in units of ln(1+concentration in mmol·m-2).

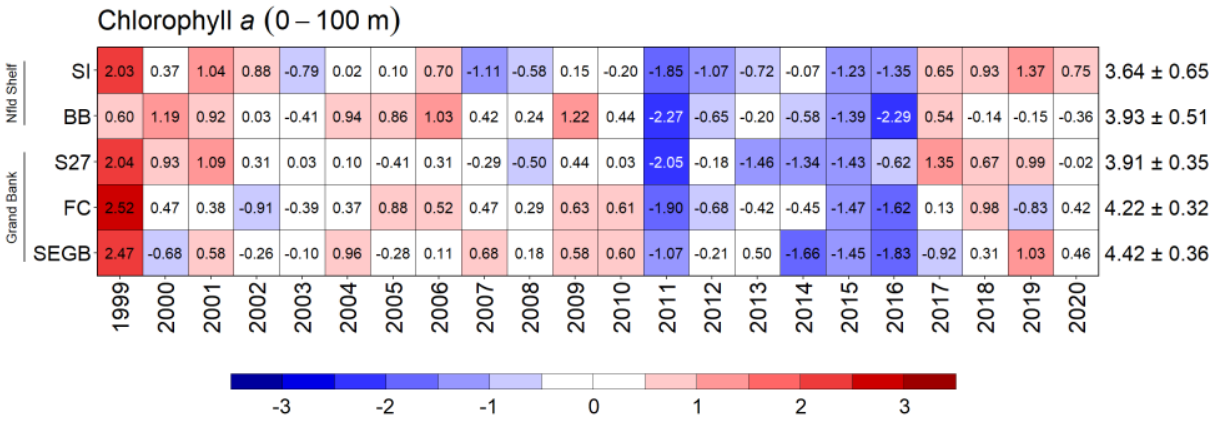

Figure 13: Annual anomaly scorecards for chlorophyll-a inventories. Numbers in cells are standardized anomalies in standard deviation (SD) units. White cells indicate near-normal conditions, i.e., ± 0.5 SD relative to the climatological mean. Blue (red) cells indicate lower (higher) concentration than normal. Grey cells indicate missing data. Climatological means and SD for the 1999-2020 reference period are listed to the right in units of ln(1+chl a biomass in mg·m-2).

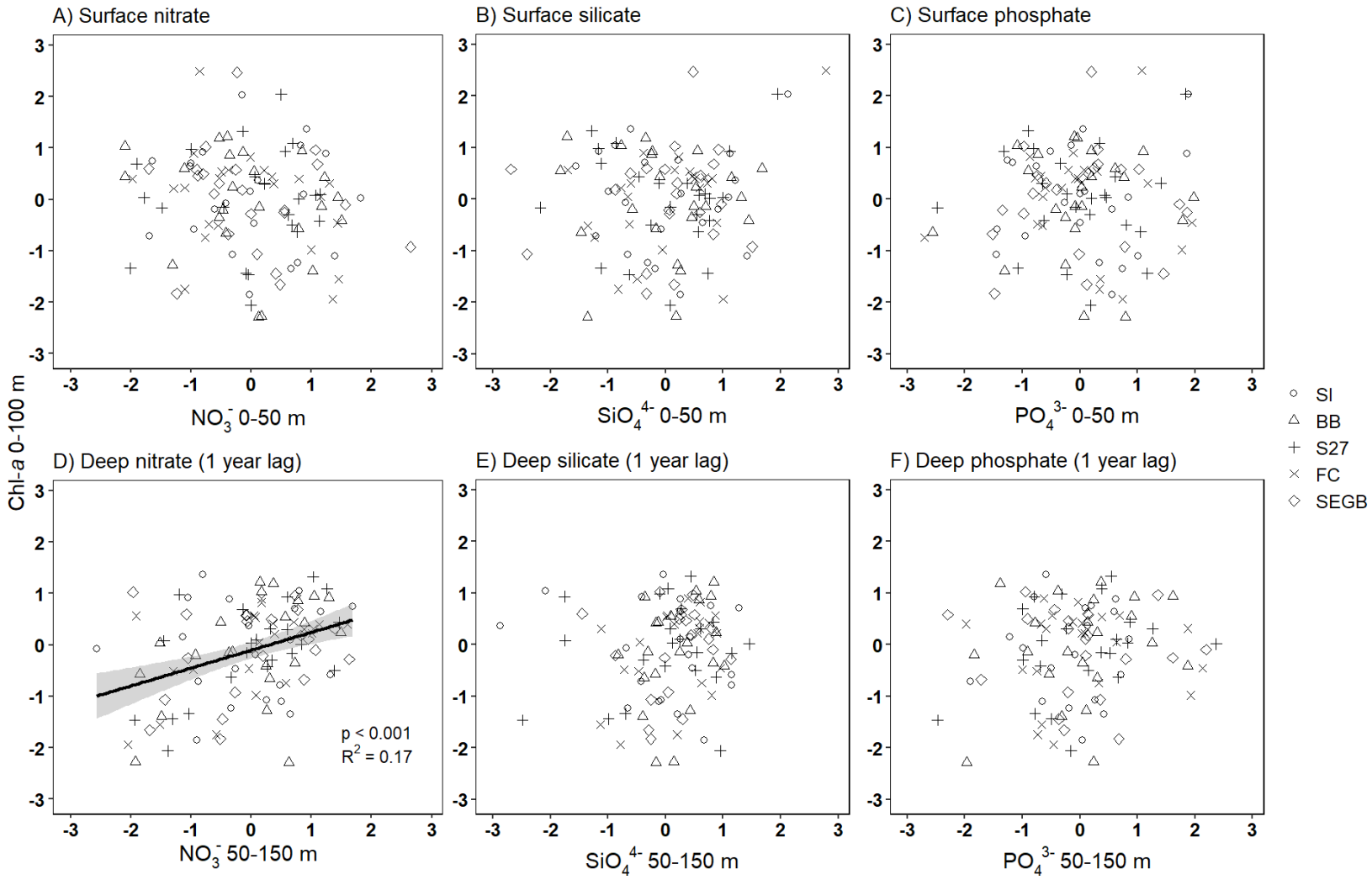

Figure 14: Linear regressions between annual anomalies of shallow (top) and 1-year lagged deep (bottom) nutrients and chlorophyll-a for the oceanographic sections Seal Island (SI), Bonavista Bay (BB), Flemish Cap (FC) and southeastern Grand Bank (SEGB), and for the high-frequency monitoring site Station 27 (S27). The fitted line (± 95% CL) indicate a significant relationship (α = 0.05). See Figure 1B for the geographic localization of the oceanographic sections and of the high-frequency monitoring site.

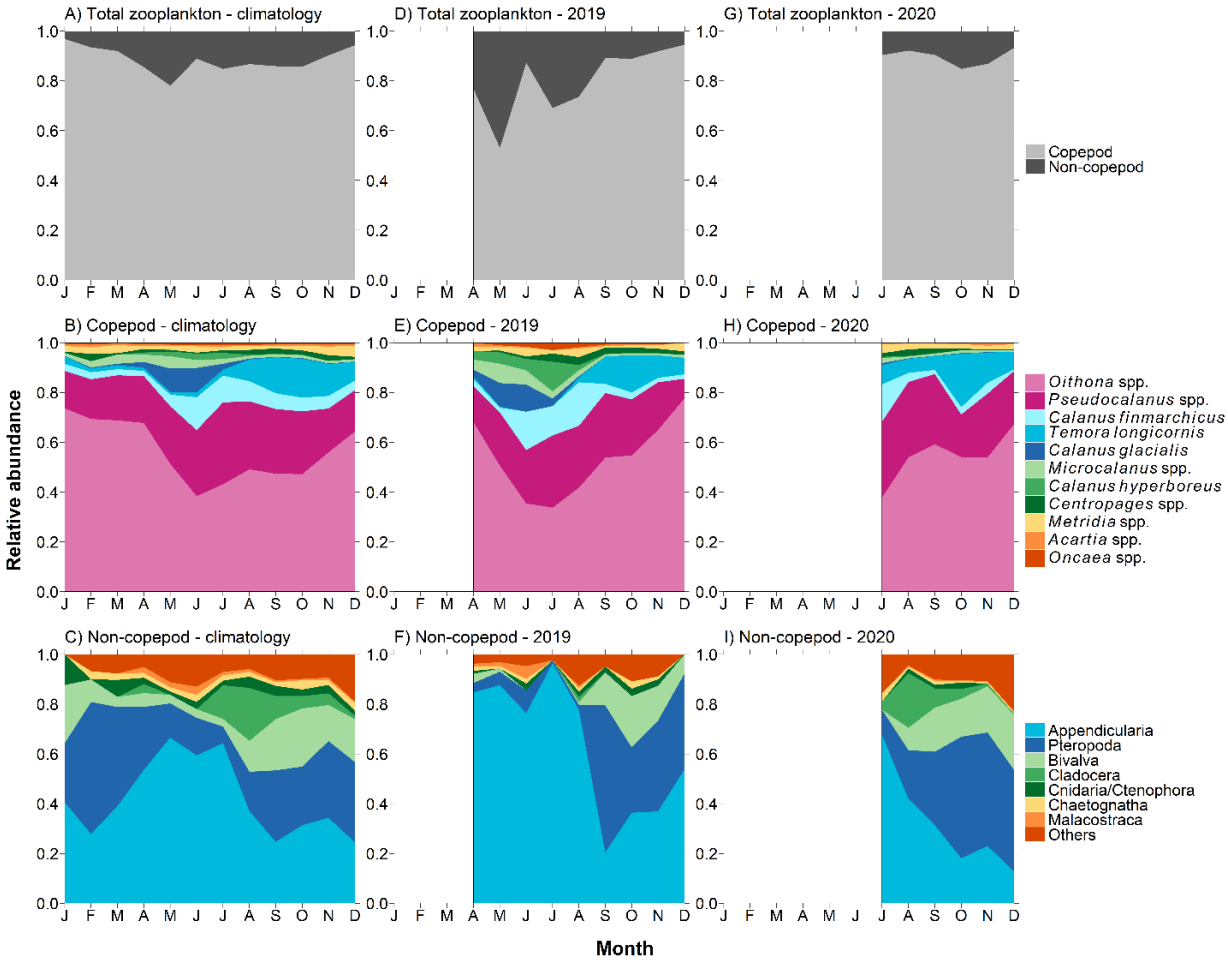

Figure 15: Relative abundances of the main mesozooplankton groups at the high-frequency monitoring site: Station 27 (S27). Relative abundance were calculated using monthly mean concentrations of the different taxa. Climatological means were calculated using a 1999–2020 reference period.

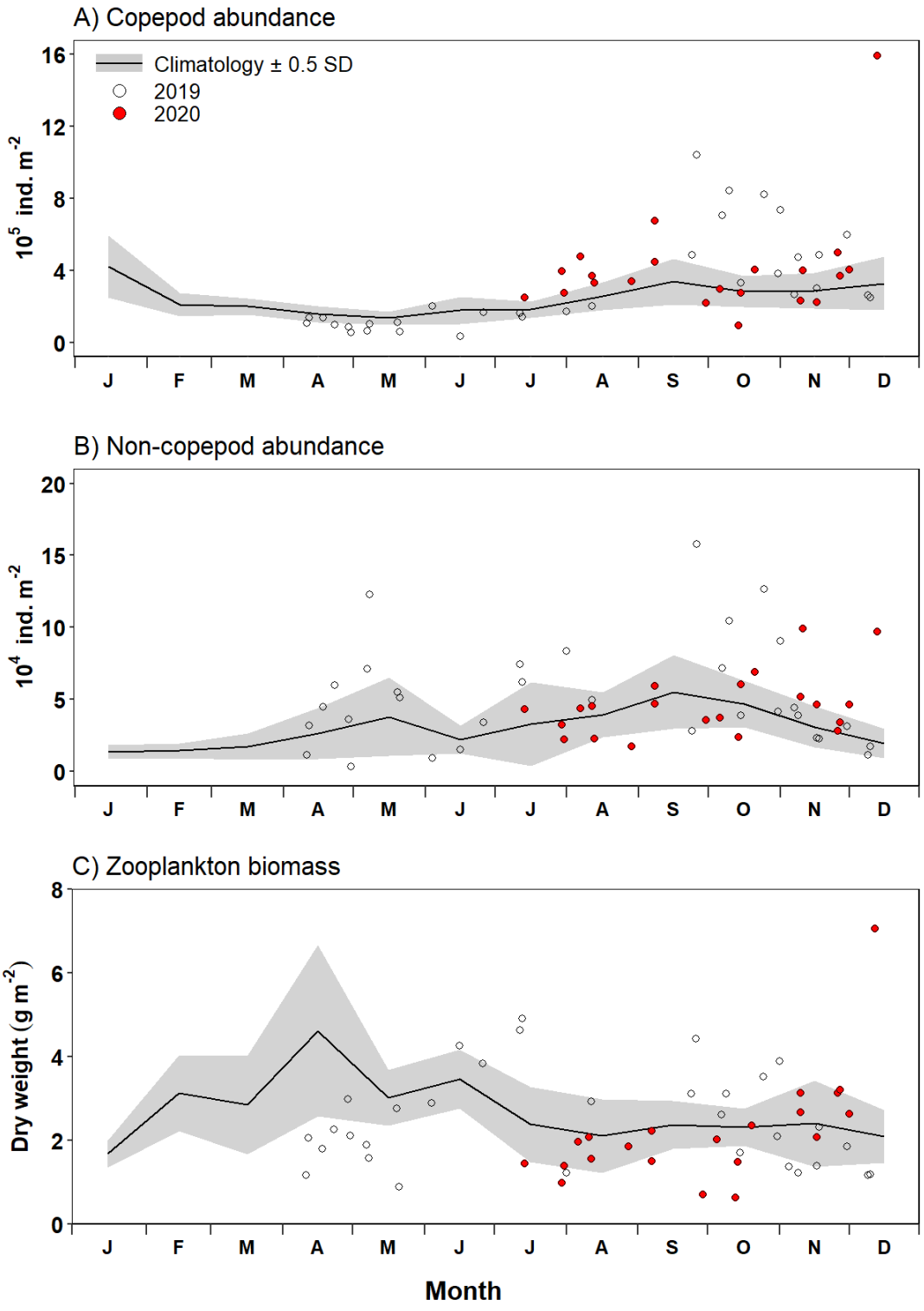

Figure 16: Seasonal variations in copepod and non-copepod abundance and total zooplankton biomass at Station 27. Black lines and grey ribbons indicate monthly means (± 0.5 SD) for the 1999–2020 reference period. Red and white circles indicate abundances during each station occupation for a given year. Abundances within ± 0.5 SD from the climatological means are considered near-normal conditions. Letters on the abscissas are months of the year.

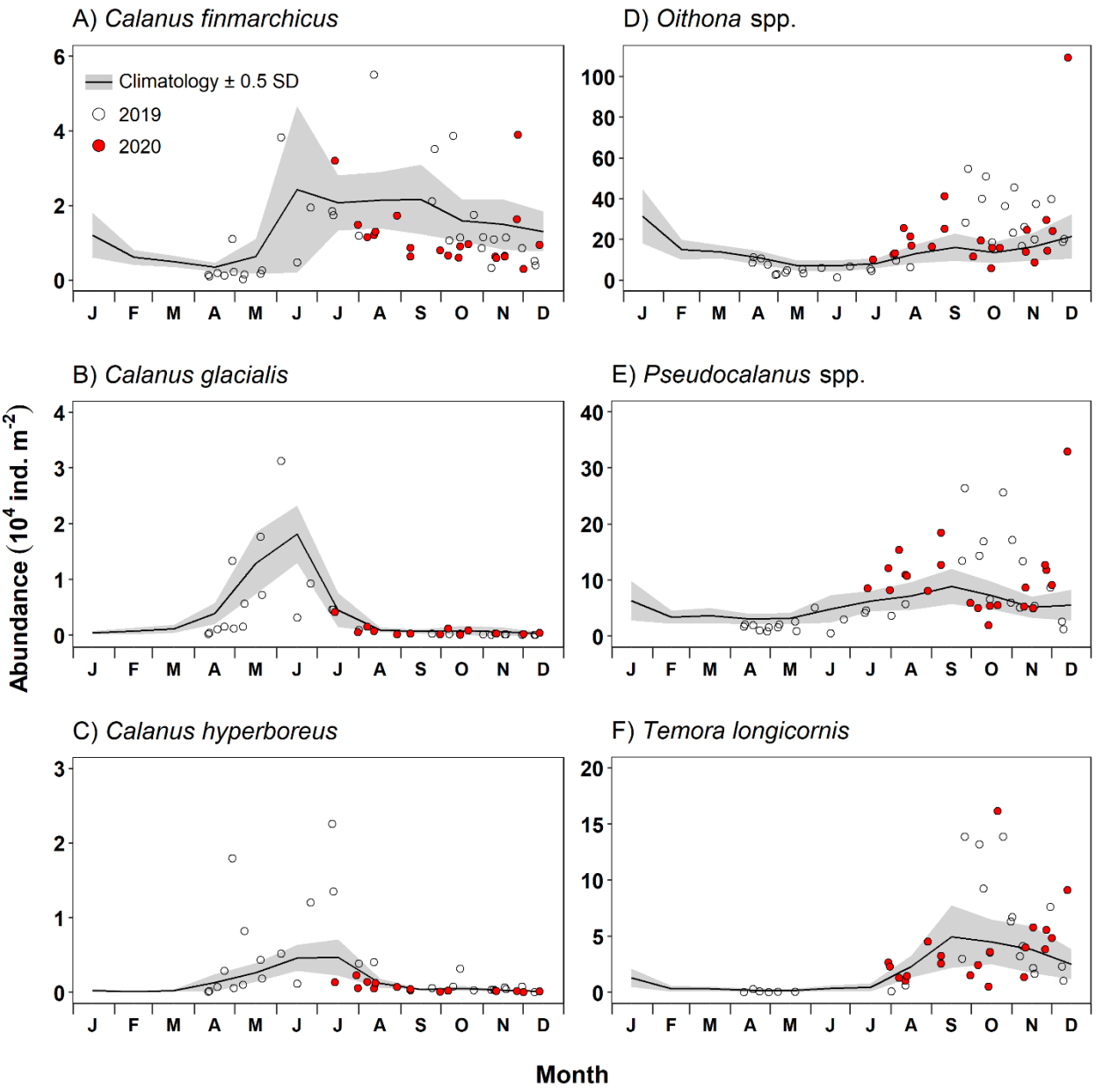

Figure 17: Seasonal variation in the abundance of ecologically important copepod taxa at Station 27. Black lines and grey ribbons indicate monthly mean abundances (± 0.5 SD) for the 1999–2020 reference period. Red and white circles indicate abundances during each station occupation for a given year. Abundances within ± 0.5 SD from the climatological means are considered near-normal conditions.

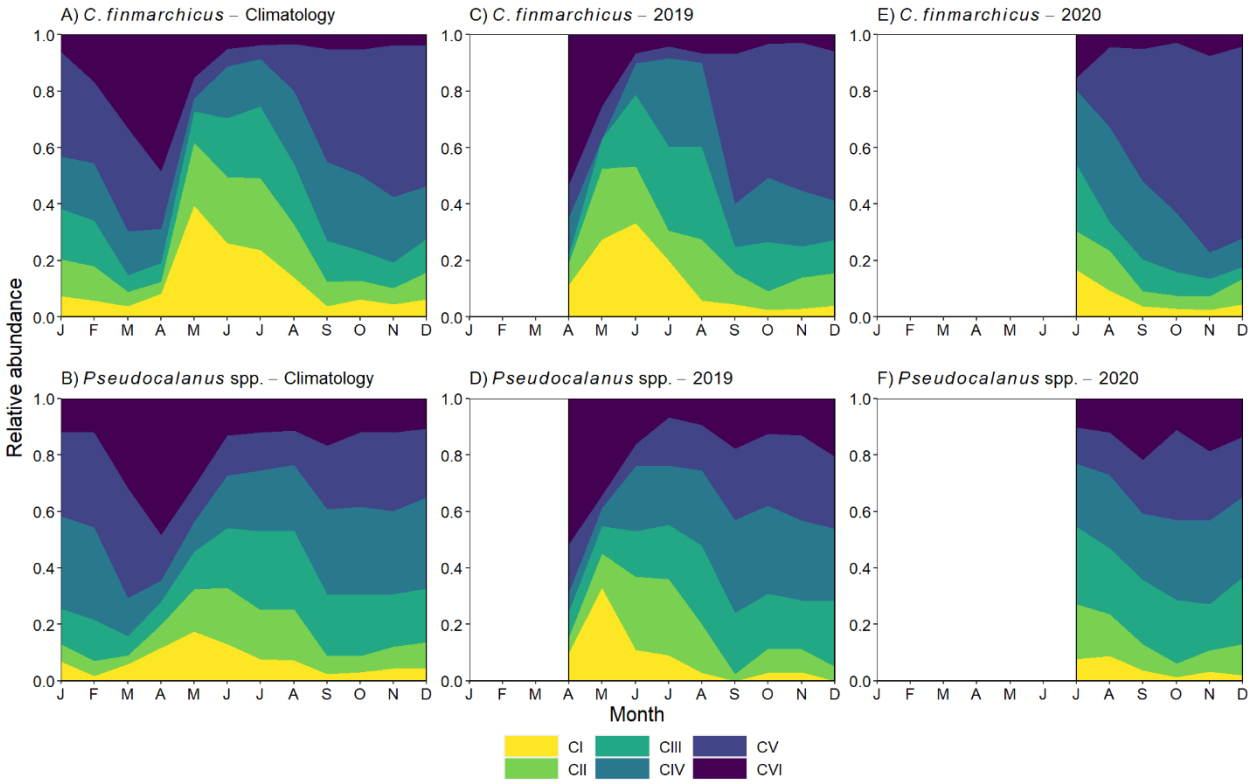

Figure 18: Seasonal variation in the relative abundance of Calanus finmarchicus (top) and Pseudocalanus spp. (bottom) copepodite stages at Station 27 for the 1999–2020 reference period and for the years 2019 and 2020. Relative abundances were calculated using monthly mean concentrations for the different copepodite stages.

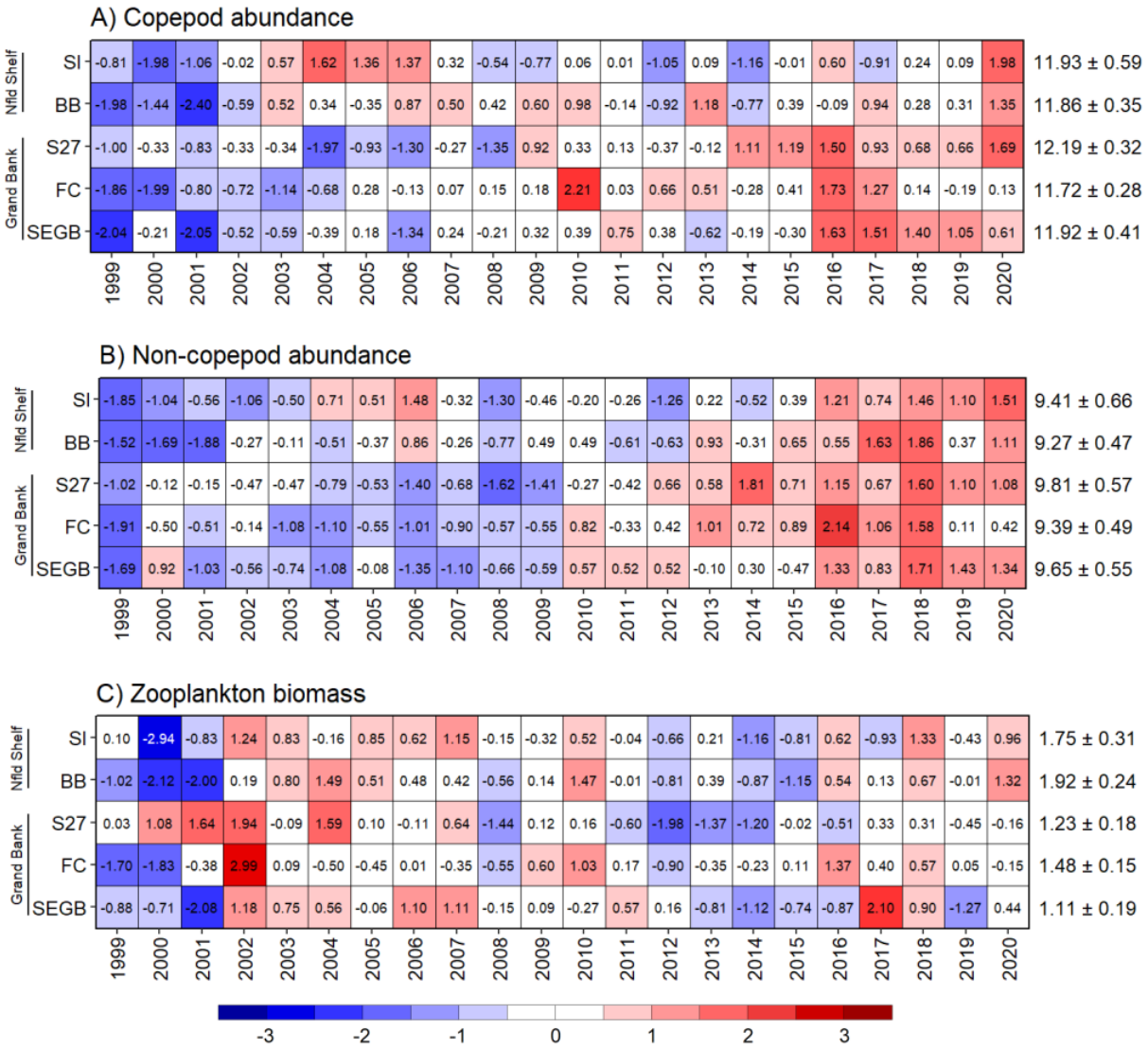

Figure 19: Annual anomaly scorecards for the abundance of copepods and non-copepods and for total zooplankton biomass. Numbers in each cell are standardized anomalies in standard deviation (SD) units. White cells indicate near-normal conditions, i.e., ± 0.5 SD relative to the climatological mean. Blue (red) cells indicate lower (higher) concentration than normal. Grey cells indicate missing data. Climatological means and SD for the 1999–2020 reference period are listed to the right in units of ln(1+individuals·m-2) for copepods and non-copepods and ln(1+biomass in g·m-2) for total zooplankton biomass.

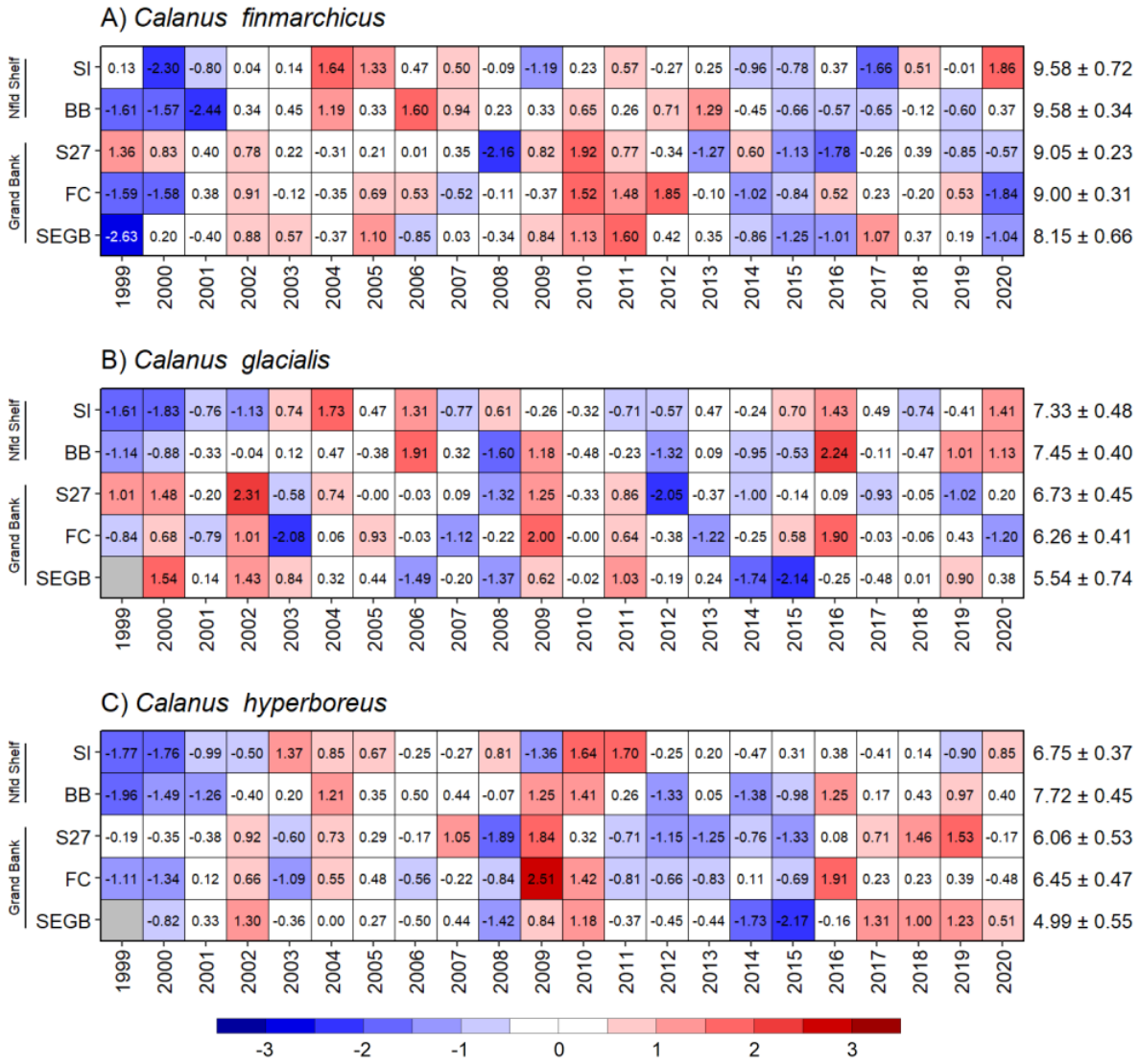

Figure 20: Annual anomaly scorecards for the abundance of large calanoid copepods. Numbers in each cell are standardized anomalies in standard deviation (SD) units. White cells indicate near-normal conditions, i.e., ± 0.5 SD relative to the climatological mean. Blue (red) cells indicate lower (higher) concentration than normal. Grey cells indicate missing data. Climatological means and SD for the 1999–2020 reference period are listed to the right in units of ln(1+individuals·m-2).

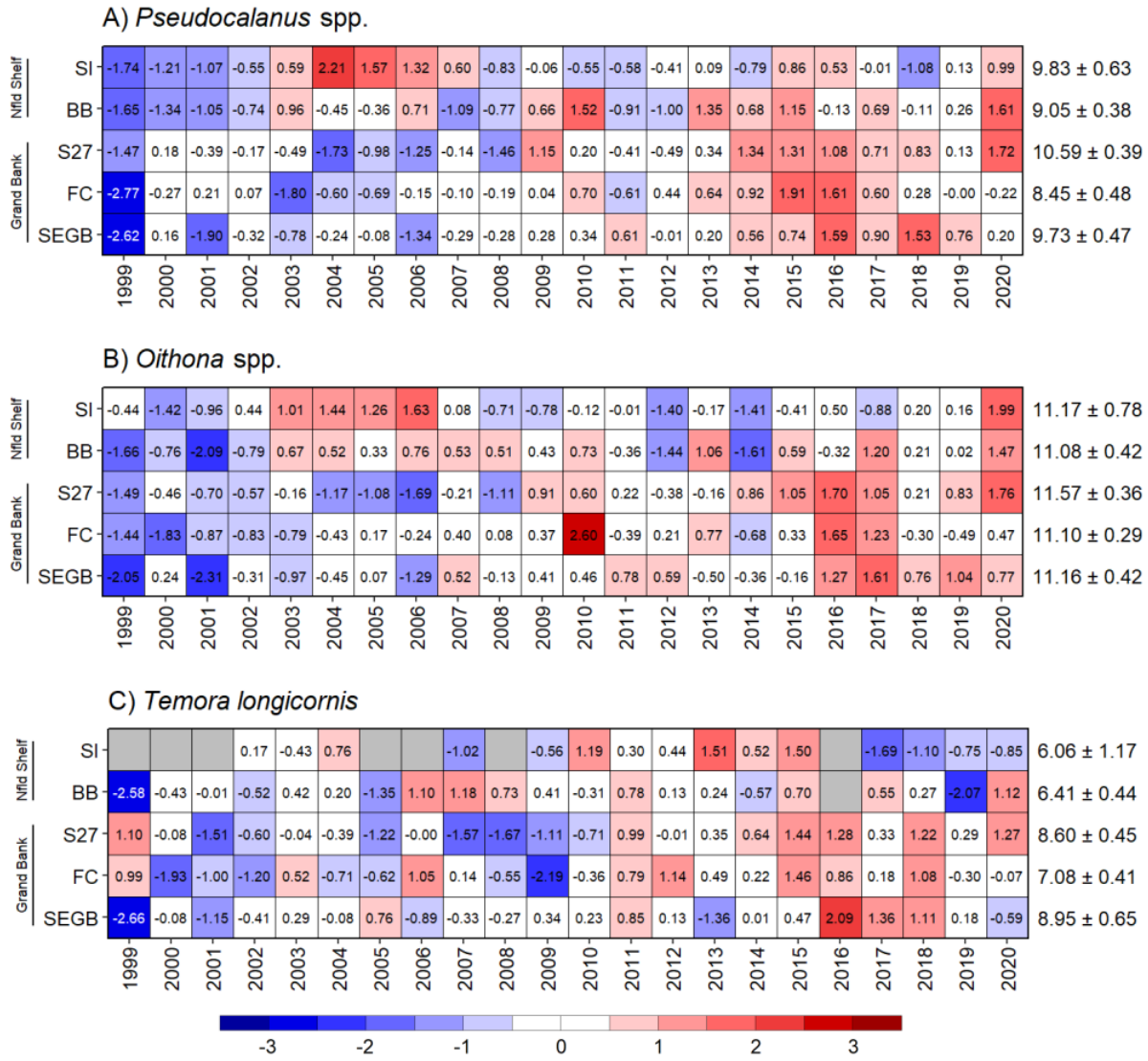

Figure 21: Annual anomaly scorecards for the abundance of dominant small copepod taxa. Numbers in each cell are standardized anomalies in standard deviation (SD) units. White cells indicate near-normal conditions, i.e., ± 0.5 SD relative to the climatological mean. Blue (red) cells indicate lower (higher) concentration than normal. Grey cells indicate missing data. Climatological means and SD for the 1999–2020 reference period are listed to the right in units of ln(1+individuals·m-2).

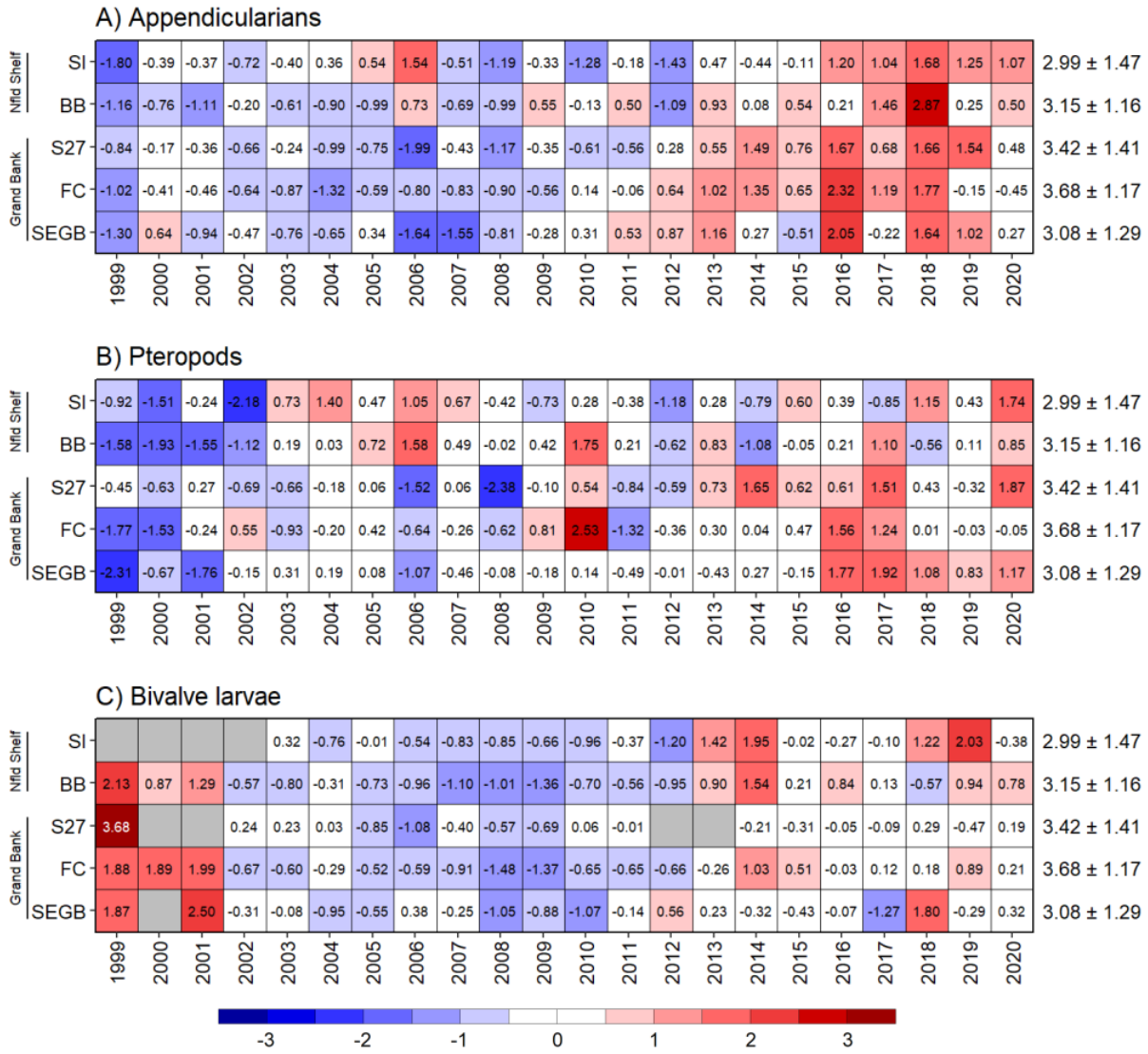

Figure 22: Annual anomaly scorecards for the abundance of dominant non-copepod zooplankton taxa. Numbers in each cell are standardized anomalies in standard deviation (SD) units. White cells indicate near-normal conditions, i.e., ± 0.5 SD relative to the climatological mean. Blue (red) cells indicate lower (higher) concentration than normal. Grey cells indicate missing data. Climatological means and SD for the 1999–2020 reference period are listed to the right in units of ln(1+individuals·m-2).

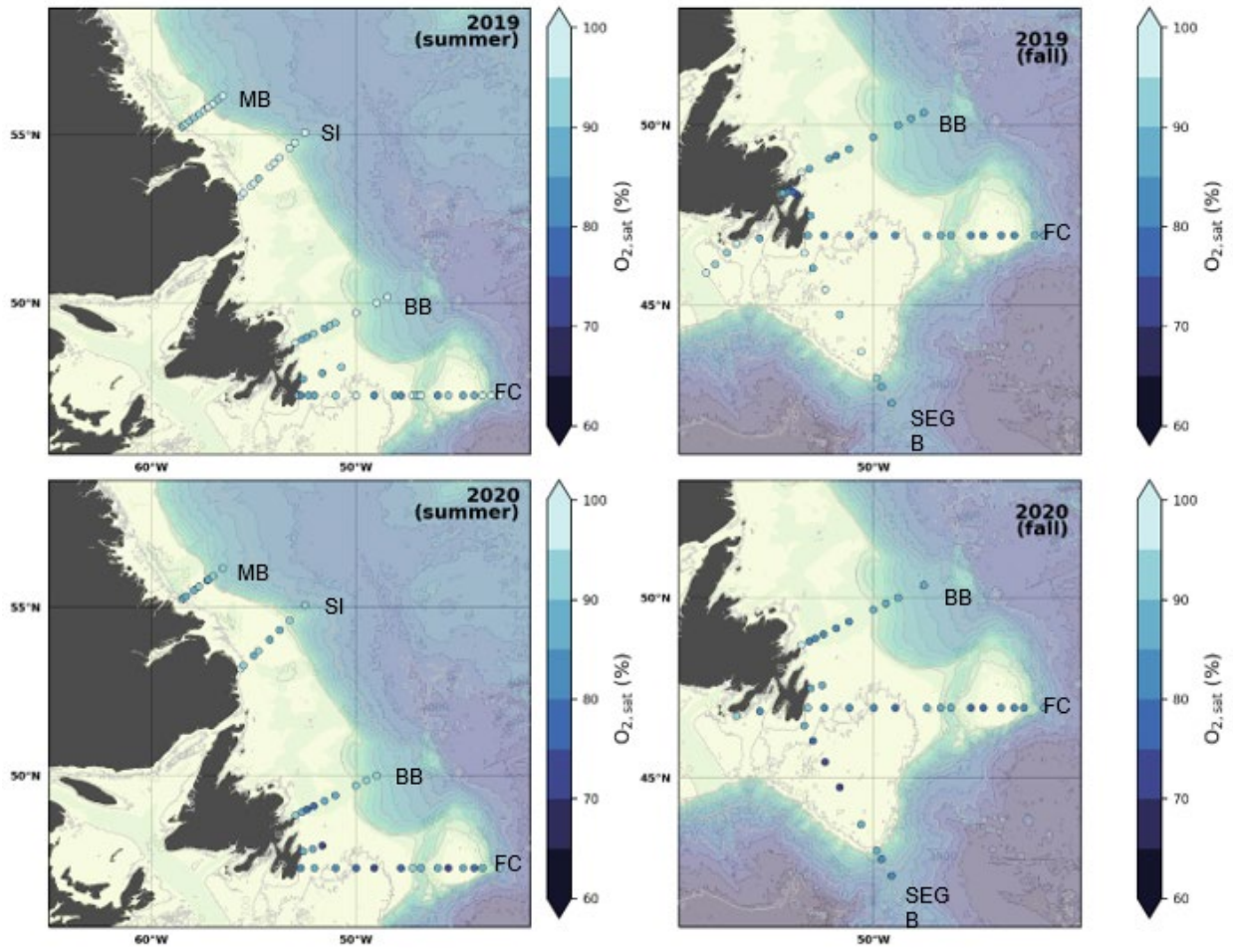

Figure 23: Summer (left) and fall (right) bottom dissolved oxygen saturation (O_2 sat) in the NL Region in 2019 (top) and 2020 (bottom) along oceanographic sections Makkovik Bank (MB), Seal Island (SI), Bonavista Bay (BB), Flemish Cap (FC) and southeastern Grand Bank (SEGB).

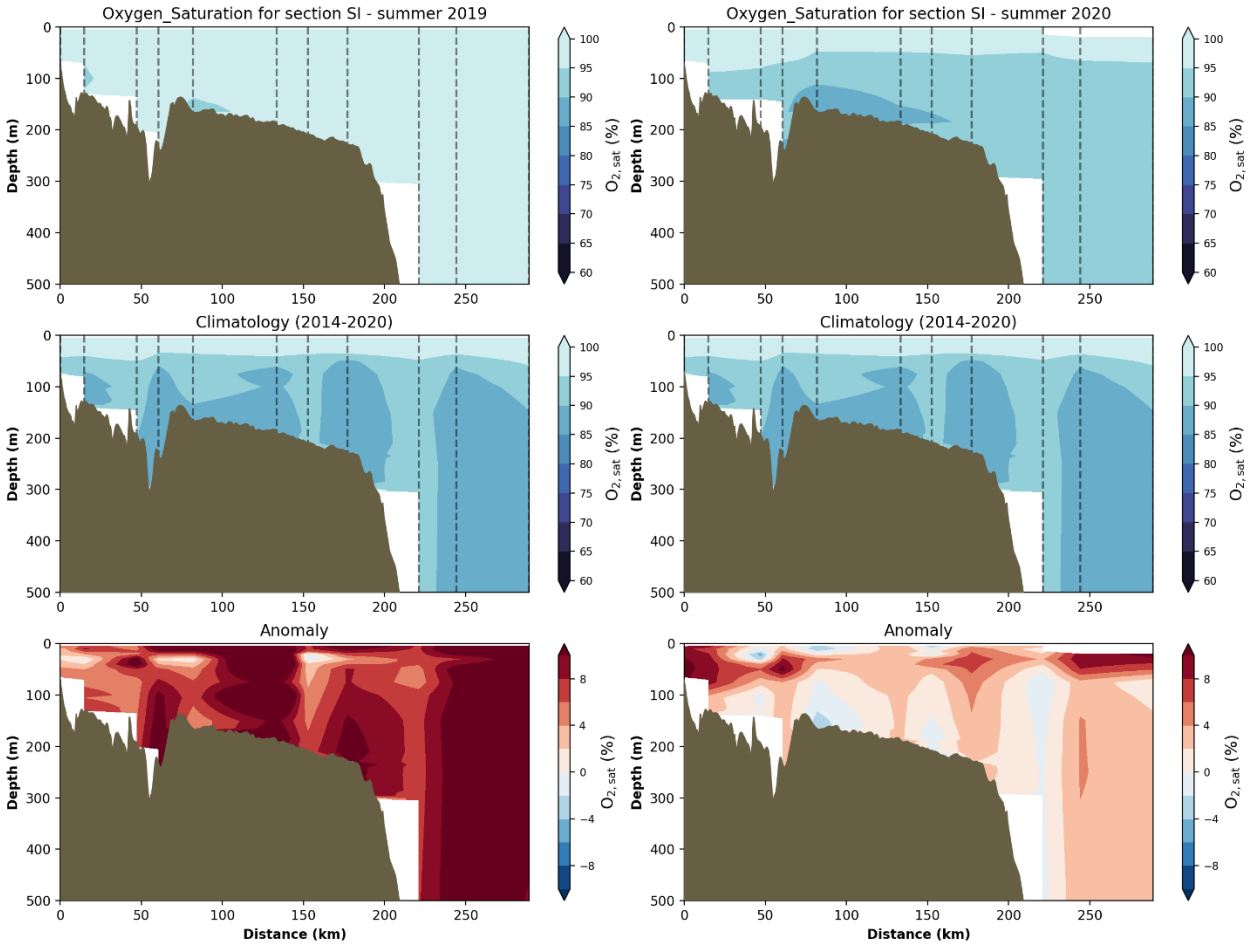

Figure 24: Summer observations (top), climatology (middle) and standardized anomalies (bottom) of bottom dissolved oxygen saturation (O_2 sat) for the Seal Island (SI) oceanographic section during 2019 (top left) and 2020 (top right). Red (blue) shades indicate O_2 sat above (below) the climatological means for the 2014–20 reference period. Vertical dashed lines indicate the location of stations along the section and their distance from shore.

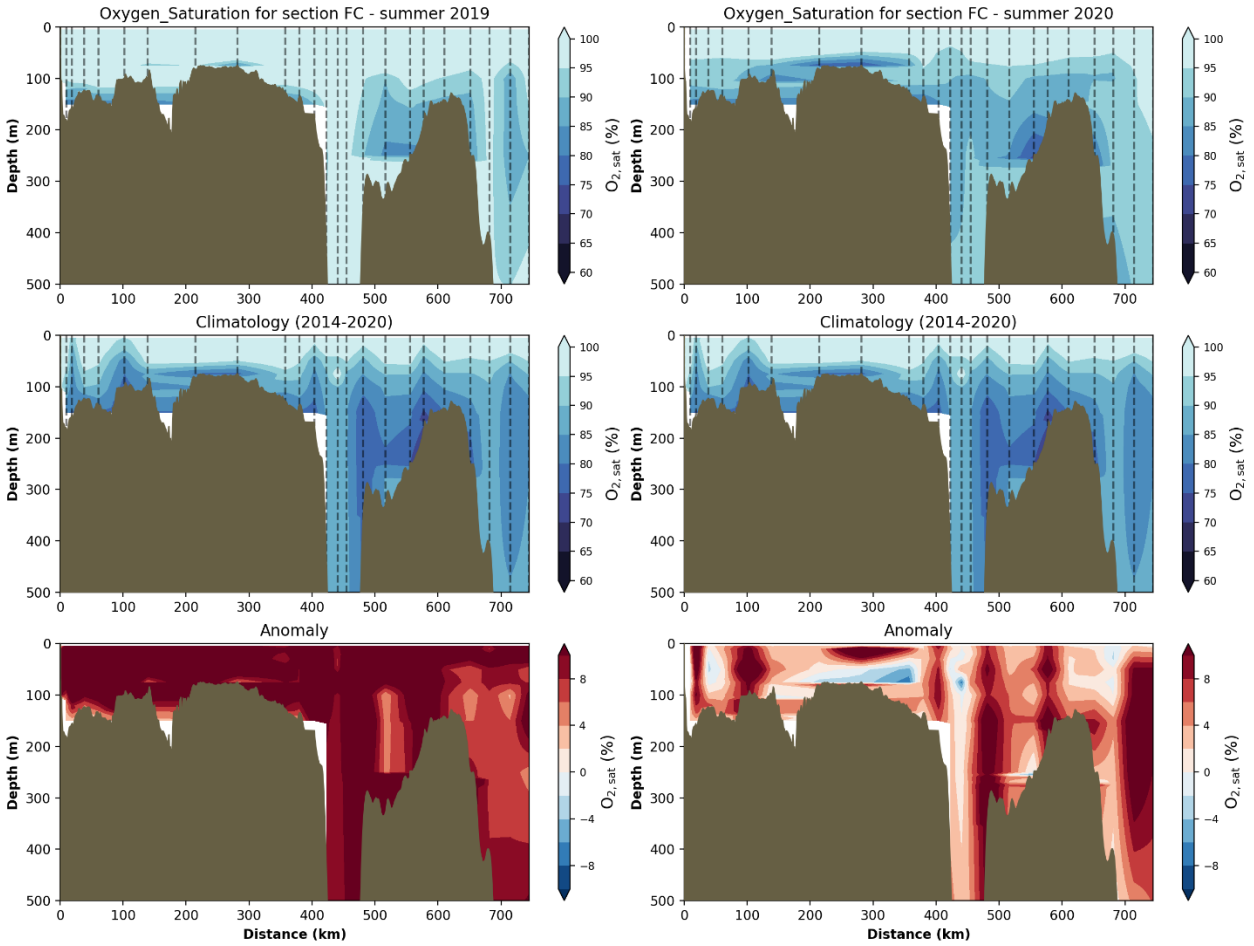

Figure 25: Summer observations (top), climatology (middle) and standardized anomalies (bottom) of bottom dissolved oxygen saturation (O_2 sat) for the Flemish Cap (FC) oceanographic section during 2019 and 2020. Blue (red) shades indicate O_2 sat below (above) the climatological means for the 2014–20 reference period. Vertical dashed lines indicate the location of the stations where water samples were collected and their distance from shore.

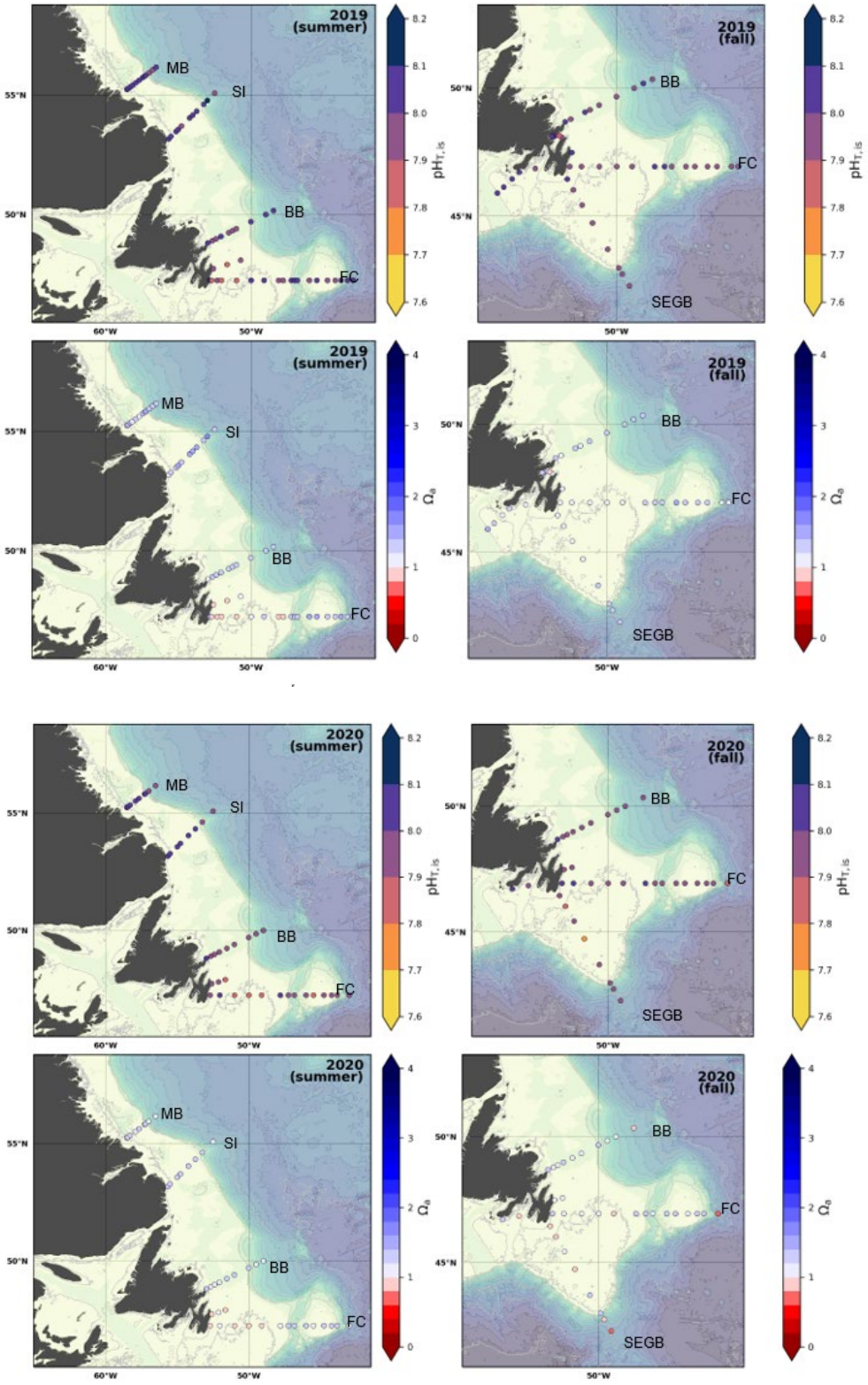

Figure 26: Summer (left) and fall (right) observations of bottom pH (top)and aragonite saturation state (Ω) (bottom) in the NL Region during 2019 (previous page) and 2020 (above) along oceanographic sections Makkovik Banks (MB), Seal Island (SI), Bonavista Bay (BB), Flemish Cap (FC), and southeastern Grand Bank (SEGB). Ω<1 indicate aragonite undersaturation.

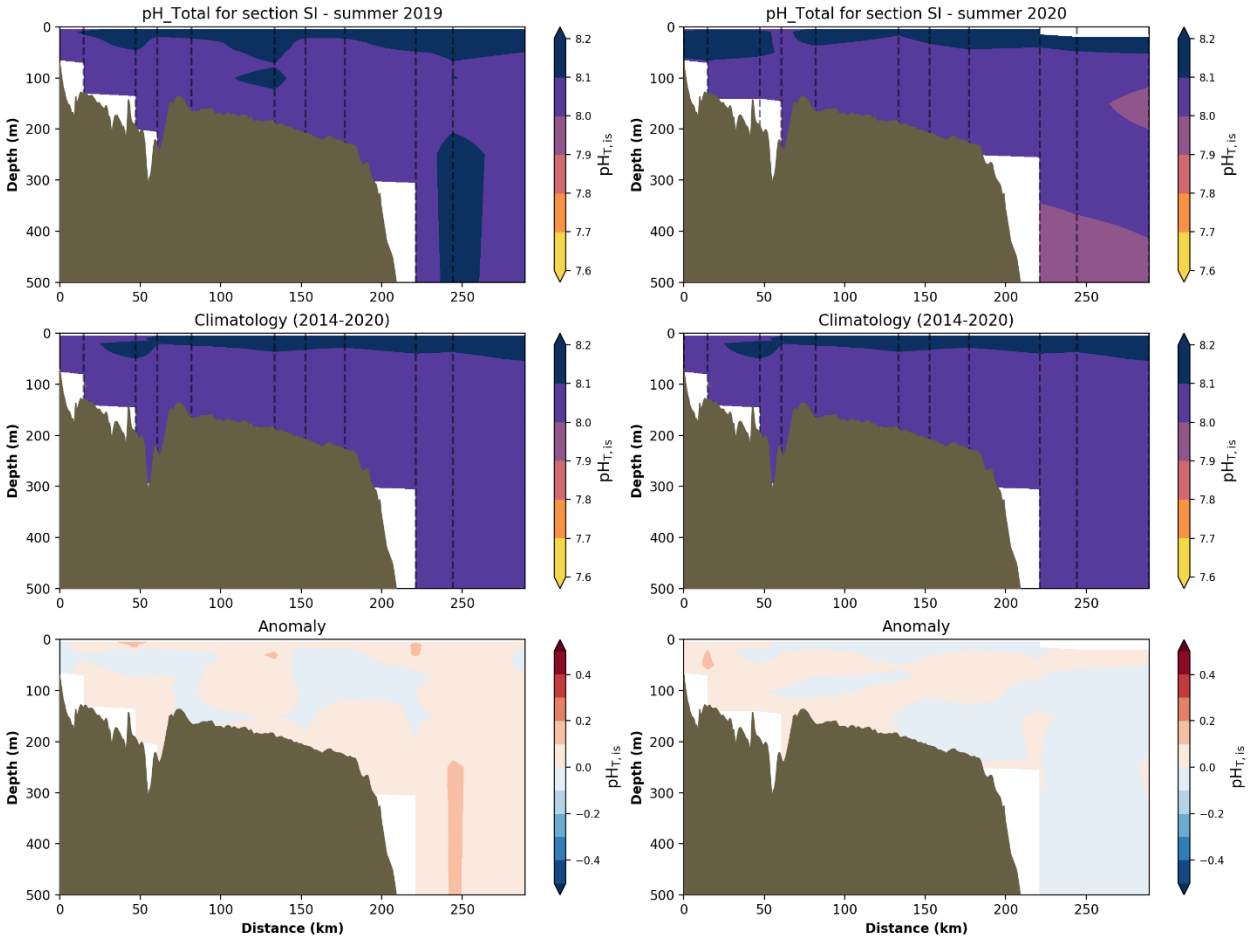

Figure 27: Summer observations (top), climatology (middle) and standardized anomalies (bottom) of pH values for the Seal Island oceanographic section during 2019 and 2020. Blue (red) shades indicate pH values below (above) the climatological means for the 2014–20 reference period. Vertical dashed lines indicate the location of the stations where samples were collected and their distance from shore.

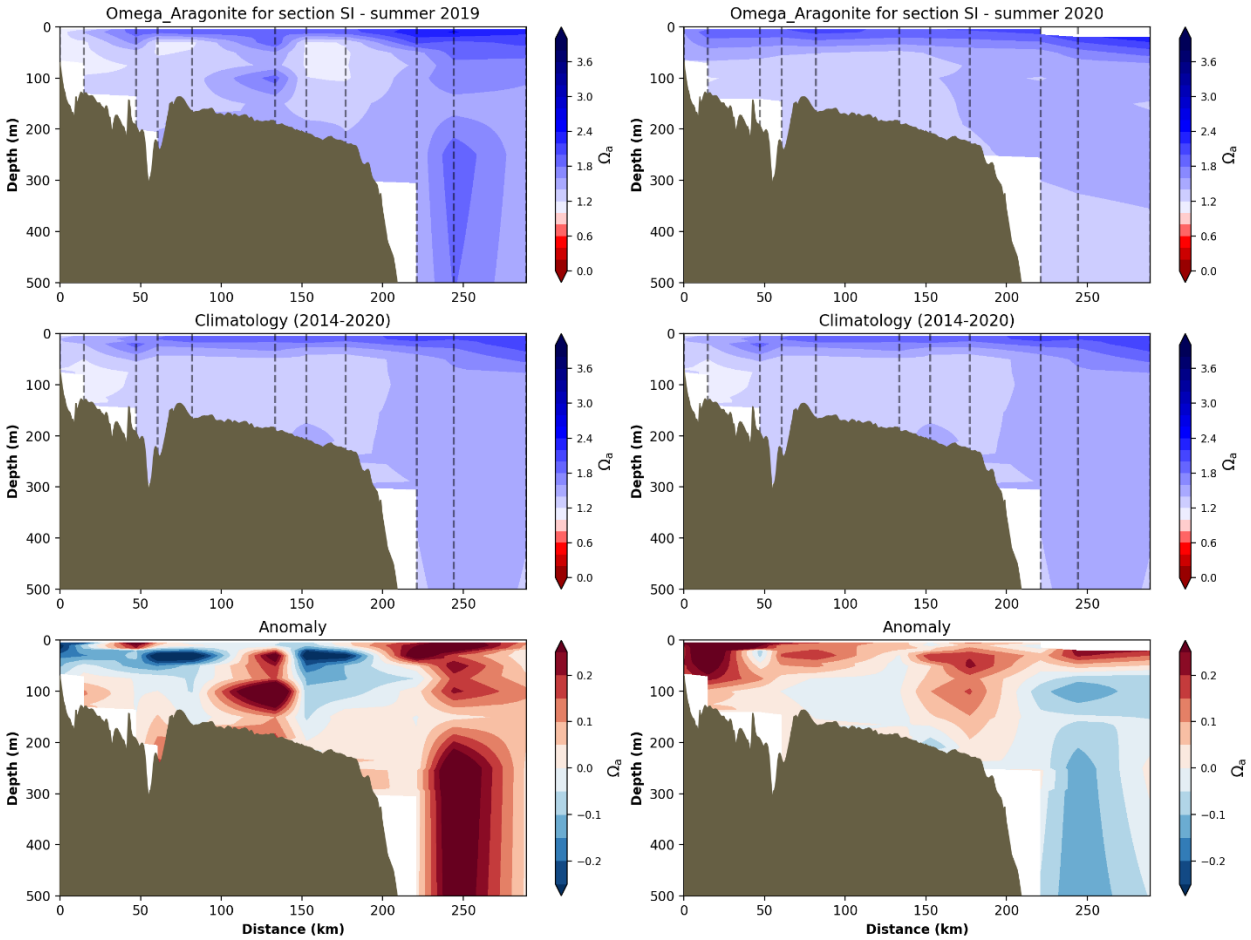

Figure 28: Summer observations of aragonite saturation state (Ω_a) values (top), climatology (middle) and standardized anomalies (bottom) for the Seal Island oceanographic section during 2019 and 2020. Blue (red) shades indicate Ω_a values below (above) the climatological means for the 2014–20 reference period. Vertical dashed lines indicate the location of the stations where samples were collected and their distance from shore.

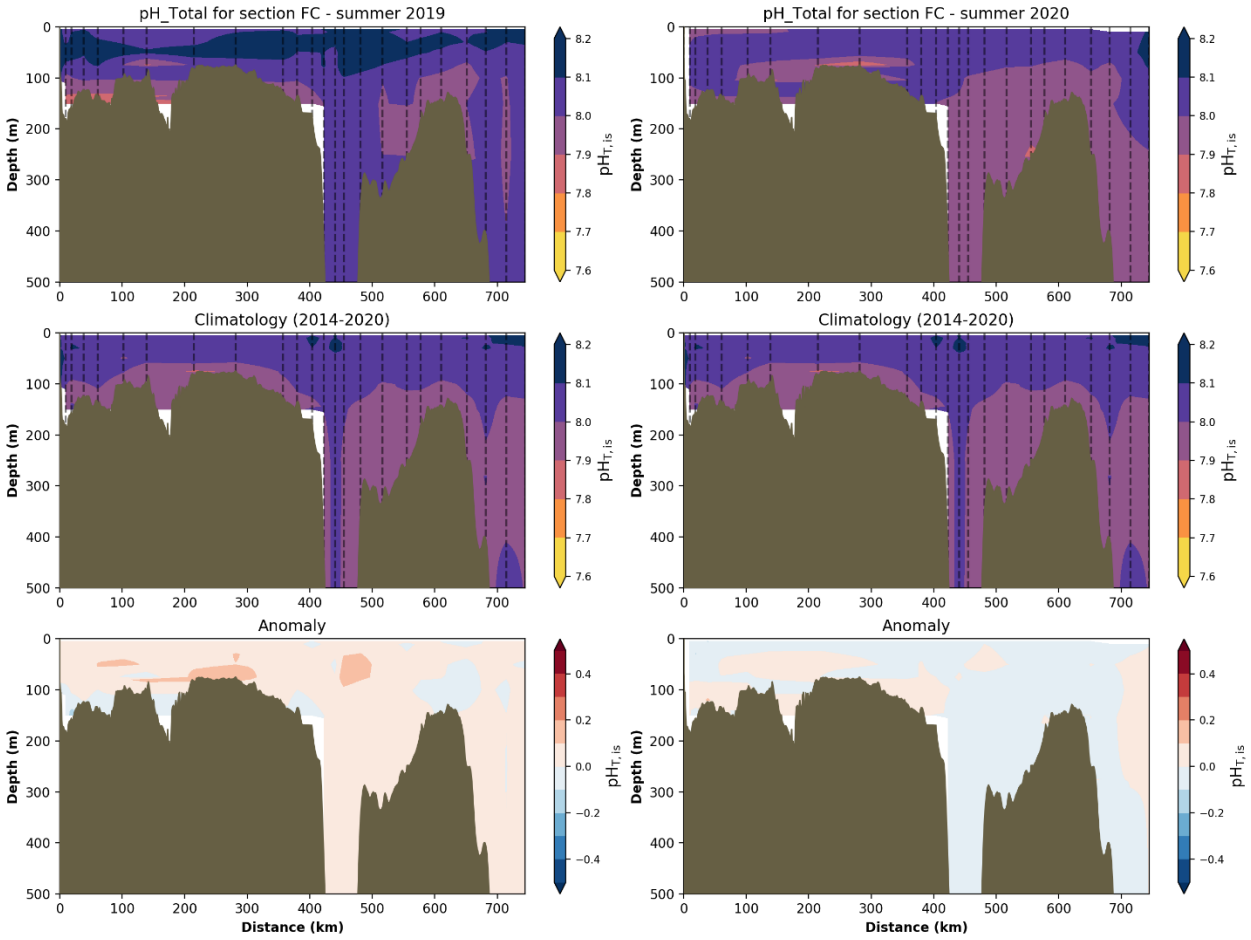

Figure 29: Summer observations of pH values (top), climatology (middle), and standardized anomalies (bottom) for the Flemish Cap (FC) oceanographic section during 2019 (left) and 2020 (right). Red (blue) anomaly shades indicate pH values above (below) the climatological means for the 2014–20 reference period. Vertical dashed lines indicate the location of the stations where samples were collected. Numbers on the abscises indicate the distance from the first near-shore station of the section.

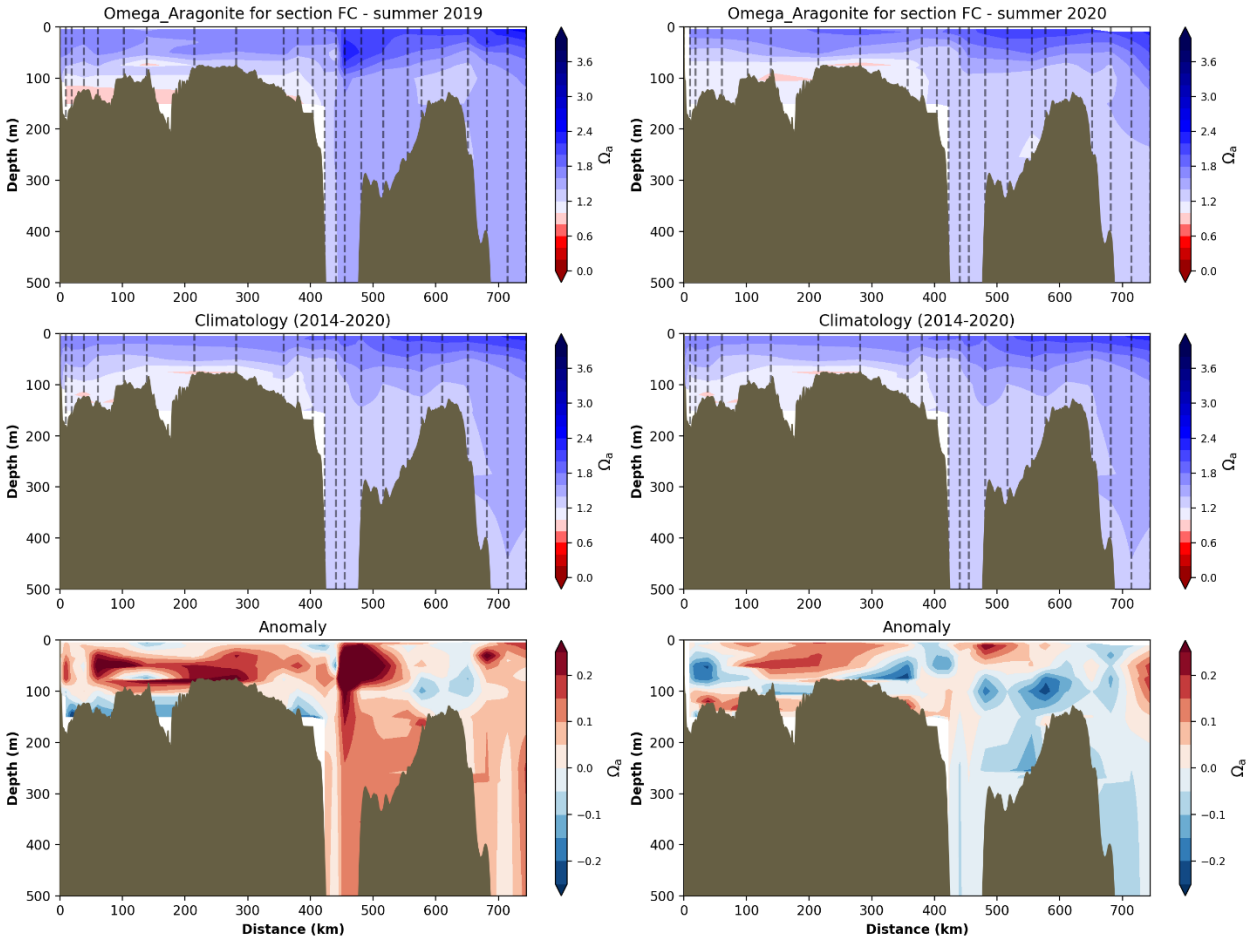

Figure 30: Summer observations of aragonite saturation state (Ω) values (top), climatology (middle) and standardized anomalies (bottom) for the Flemish Cap (FC) oceanographic section during 2019 (left) and 2020 (right). Red (blue) anomaly shades indicate Ω values above (below) the climatological means for the 2014–20 reference period. Vertical dashed lines indicate the location of the stations where samples were collected. Numbers on the abscises indicate the distance from the first near-shore station of the section.